1

Changes to Carbon Isotopes in Atmospheric CO₂ over the Industrial Era and into the Future

4

5

6

7

Heather Graven[1,2], Ralph F. Keeling[3] and Joeri Rogelj[2,4]

[1]Department of Physics, Imperial College London, London, UK.

[2]Grantham Institute for Climate Change and the Environment, Imperial College London, London, UK.

[3]Scripps Institution of Oceanography, University of California, San Diego, USA.

[4]ENE Program, International Institute for Applied Systems Analysis, Laxenburg, Austria.

14

Corresponding author: Heather Graven (h.graven@imperial.ac.uk)

16

Key Points:

- Carbon isotopes, ^{14}C and ^{13}C, in atmospheric CO₂ are changing in response to fossil fuel emissions and other human activities

- Future simulations using different SSPs show continued changes in isotopic ratios that depend on fossil fuel emissions and, for ^{13}C, BECCS

- Applications using atmospheric ^{14}C and ^{13}C in studies of the carbon cycle or other fields will be affected by future changes

24

25 **Abstract (up to 500 words)**

26   In this "Grand Challenges" paper, we review how the carbon isotopic composition of
27   atmospheric CO_2 has changed since the Industrial Revolution due to human activities and their
28   influence on the natural carbon cycle and we provide new estimates of possible future changes
29   for a range of scenarios. Emissions of CO_2 from fossil fuel combustion and land use change
30   reduce the ratio of $^{13}C/^{12}C$ in atmospheric CO_2 ($\delta^{13}CO_2$). This is because ^{12}C is preferentially
31   assimilated during photosynthesis and $\delta^{13}C$ in plant-derived carbon in terrestrial ecosystems and
32   fossil fuels is lower than atmospheric $\delta^{13}CO_2$. Emissions of CO_2 from fossil fuel combustion also
33   reduce the ratio of $^{14}C/C$ in atmospheric CO_2 ($\Delta^{14}CO_2$) because ^{14}C is absent in million-year-old
34   fossil fuels, which have been stored for much longer than the radioactive decay time of ^{14}C.
35   Atmospheric $\Delta^{14}CO_2$ rapidly increased in the 1950s-60s because of ^{14}C produced during nuclear
36   bomb testing. The resulting trends in $\delta^{13}C$ and $\Delta^{14}C$ in atmospheric CO_2 are influenced not only
37   by these human emissions, but also by natural carbon exchanges that mix carbon between the
38   atmosphere and ocean and terrestrial ecosystems. This mixing caused $\Delta^{14}CO_2$ to return towards
39   preindustrial levels in the first few decades after the spike from nuclear testing. More recently, as
40   the bomb ^{14}C excess is now mostly well mixed with the decadally-overturning carbon reservoirs,
41   fossil fuel emissions have become the main factor driving further decreases in atmospheric
42    $\Delta^{14}CO_2$. For $\delta^{13}CO_2$, in addition to exchanges between reservoirs, the extent to which ^{12}C is
43   preferentially assimilated during photosynthesis appears to have increased, slowing down the
44   recent $\delta^{13}CO_2$ trend slightly. A new compilation of ice core and flask $\delta^{13}CO_2$ observations
45   indicates that the decline in $\delta^{13}CO_2$ since the preindustrial period is less than some prior
46   estimates, which may have incorporated artifacts owing to offsets from different laboratories'
47   measurements.

48   Atmospheric observations of $\delta^{13}CO_2$ have been used to investigate carbon fluxes and the
49   functioning of plants, and they are used for comparison with $\delta^{13}C$ in other materials such as tree
50   rings. Atmospheric observations of $\Delta^{14}CO_2$ have been used to quantify the rate of air-sea gas
51   exchange and ocean circulation, and the rate of net primary production and the turnover time of
52   carbon in plant material and soils. Atmospheric observations of $\Delta^{14}CO_2$ are also used for
53   comparison with $\Delta^{14}C$ in other materials in many fields such as archaeology, forensics and
54   physiology. Another major application is the assessment of regional emissions of CO_2 from
55   fossil fuel combustion using $\Delta^{14}CO_2$ observations and models.

56   In the future, $\delta^{13}CO_2$ and $\Delta^{14}CO_2$ will continue to change. The sign and magnitude of the
57   changes are mainly determined by global fossil fuel emissions. We present here simulations of
58   future $\delta^{13}CO_2$ and $\Delta^{14}CO_2$ for six scenarios based on the shared socioeconomic pathways (SSPs)
59   from the 6th Coupled Model Intercomparison Project (CMIP6). Applications using atmospheric
60    $\delta^{13}CO_2$ and $\Delta^{14}CO_2$ observations in carbon cycle science and many other fields will be affected
61   by these future changes. We recommend an increased effort toward making coordinated
62   measurements of $\delta^{13}C$ and $\Delta^{14}C$ across the Earth System, and for further development of isotopic
63   modelling and model-data analysis tools.

64

65 **1. Introduction**

66   Carbon isotopes are present in the atmosphere, ocean and terrestrial biosphere in ratios of
67   approximately 99% $^{12}C/C$, 1% $^{13}C/C$ and 1×10^{-12} $^{14}C/C$. ^{12}C and ^{13}C are stable isotopes while ^{14}C

68   is a radioactive isotope called radiocarbon. Radiocarbon is formed naturally in the upper
69   atmosphere from cosmogenic radiation, which produces neutrons that react with atmospheric
70   nitrogen. Because the isotopic composition of carbon is affected by physical, chemical and
71   biological processes, these ratios are not constant and they vary across different carbon pools and
72   over time and space. Precise measurements of small differences in these ratios, together with
73   theoretical or empirical models of isotopic fractionation and mixing, enable the investigation of
74   various aspects of the carbon cycle. Observing and analyzing the changes in carbon isotopic
75   composition of atmospheric CO_2 can help to understand the natural carbon cycle's response to
76   human activities.

77   The notation $\delta^{13}C$ refers to the deviation of the ratio $^{13}C/^{12}C$ in a sample from a standard ratio
78   $^{13}C/^{12}C$, referred to as Vienna Pee Dee Belemnite (VPDB). Typical measurement precision is
79   ±0.01-0.03 ‰ for atmospheric CO_2. The primary international reference material for $\delta^{13}C$ is
80   calcite (IAEA-603 and, formerly, NBS19). Calcite must be converted to CO_2 to implement the
81   VPDB scale at individual laboratories, which has been shown to result in significant laboratory
82   offsets [*WMO/IAEA*, 2003]. Current activities to address measurement compatibility include the
83   distribution of pure CO_2 or CO_2 in whole air reference materials [*Brand et al.*, 2009; *Wendeberg*
84   *et al.*, 2013; *WMO/IAEA*, 2018], but achieving long-term compatibility of $\delta^{13}C$ measurements in
85   atmospheric CO_2 made at different laboratories remains a challenge and laboratory offsets must
86   be considered when compiling data (see Section 5).

87   The notation used for ^{14}C is $\Delta^{14}C$, which is similar to the definition of $\delta^{13}C$ in that it refers to
88   deviations from a standard ratio termed "Modern". The notation $\Delta^{14}C$ includes a correction for
89   radioactive decay in samples of known age and a correction for mass-dependent fractionation,
90   defined as Δ in *Stuiver and Polach* [1977]. Assuming that any process discriminating against ^{13}C
91   will discriminate approximately twice as strongly against ^{14}C, measurements of $\delta^{13}C$ in a sample
92   can be used to correct for mass-dependent fractionation. This enables $\Delta^{14}C$ to uncover effects
93   that are unrelated to simple fractionation processes. Typical measurement precision is ±2-3 ‰
94   for atmospheric CO_2. Reference material used for $\Delta^{14}C$ measurements is typically oxalic acid
95   [*Stuiver*, 1983] but whole air reference materials have also been used for atmospheric
96   measurements [*Graven et al.*, 2012b]. Whole air and CO_2 have been used in intercomparisons
97   between radiocarbon laboratories making atmospheric measurements and generally showed
98   compatibility of 2 ‰ or better [*Hammer et al.*, 2017; *Miller et al.*, 2013], in addition to
99   intercomparison activities using wood cellulose and other materials (e.g. [*Scott et al.*, 2010]).

100   In this paper, we review the observed changes in the ^{13}C and ^{14}C isotopic composition of
101   atmospheric CO_2 ($\delta^{13}CO_2$ and $\Delta^{14}CO_2$) over the Industrial Period and the processes driving these
102   changes. We review key applications for atmospheric $\delta^{13}CO_2$ and $\Delta^{14}CO_2$ observations from the
103   literature, with an emphasis on global or large-scale processes. Then we present new simulations
104   of future changes in atmospheric $\delta^{13}CO_2$ and $\Delta^{14}CO_2$ corresponding to future emission scenarios
105   through 2100. We discuss the impacts of these future changes on applications for atmospheric
106   $\delta^{13}CO_2$ and $\Delta^{14}CO_2$ observations and make recommendations for observational and modelling
107   activities for $\delta^{13}C$ and $\Delta^{14}C$.

108

2. The ^{14}C and ^{13}C Suess Effects

110   The onset of the Industrial Revolution initiated extensive fossil fuel burning that introduced
111   carbon previously stored in geological reservoirs into the atmosphere. Fossil fuels are completely

112 devoid of ^{14}C because they have been stored in geological reservoirs for millions of years, much
113 longer than the ^{14}C half-life of 5700 years. This gives fossil fuels a Δ^{14}C signature of -1000 ‰.
114 For ^{13}C, the carbon in fossil fuels has an isotopic signature (δ^{13}C) that ranges from -44 to -19 ‰
115 [*Andres et al.*, 2000]. The δ^{13}C in fossil fuels is lower than the δ^{13}C in atmospheric CO_2 (-8.5 to -
116 4 ‰ from the present through the past 65 million years [*Graven et al.*, 2017; *Tipple et al.*, 2010])
117 because fossil fuel carbon originates from plant materials and the photosynthesis process
118 discriminates against ^{13}C. There are also geological processes causing further discrimination
119 against ^{13}C for some fossil fuels. There is no fractionation during combustion if combustion is
120 complete, but carbonization can produce fractionation [*Turney et al.*, 2006].

121 As fossil fuels are slightly depleted in ^{13}C and entirely depleted in ^{14}C, the burning of fossil fuels
122 increases $^{12}CO_2$ at a faster relative rate than $^{13}CO_2$ and $^{14}CO_2$. This dilution effect, which drives
123 δ^{13}C and Δ^{14}C downwards, is termed "The Suess Effect." In 1955, Hans Suess published the
124 first observations of ^{14}C dilution using tree ring records of atmospheric CO_2 [*Suess*, 1955]. The
125 "Suess Effect" terminology was also later applied to ^{13}C, as the dilution process is similar
126 [*Keeling*, 1979]. Importantly, the decreases observed in atmospheric $\delta^{13}CO_2$ and $\Delta^{14}CO_2$ are
127 governed not only by the amount of fossil fuels burnt, but also by other human activities and by
128 natural carbon cycle exchanges and their response to changes in atmospheric composition and
129 climate.

130 Cement manufacturing also involves "fossil" carbon in that the source material is geological and
131 therefore free of any ^{14}C. The source material is carbonate rock, which has a δ^{13}C of
132 approximately 0 ‰. The amount of CO_2 produced by cement manufacturing is only a few
133 percent of the CO_2 produced by fossil fuel burning. The global average δ^{13}C for all fossil fuel
134 combustion and cement production has been -28 to -24 ‰ [*Andres et al.*, 2016]. It has shifted
135 toward more negative values in recent years as the share of combustion from natural gas (δ^{13}C ~
136 -44 ‰) increases while coal (δ^{13}C ~ -24 ‰) decreases.

137 Land use changes represent another influence on the carbon cycle from human activities. Land
138 use can have various effects that could impact $\delta^{13}CO_2$ and $\Delta^{14}CO_2$: net transfer of carbon from
139 the biosphere to the atmosphere (or vice versa), changes to the average ^{13}C discrimination and its
140 spatial pattern through changes in plant type such as the conversion of forest to pasture, and
141 changes in the residence time of carbon in the biosphere. Overall, land use appears to have had
142 small effects on global mean $\delta^{13}CO_2$ and $\Delta^{14}CO_2$ over the Industrial Period, in part because of
143 responses of natural biospheric and ocean fluxes that compensate for land use effects on $\delta^{13}CO_2$
144 and $\Delta^{14}CO_2$. However, land use effects could be important regionally and for some applications
145 [*Scholze et al.*, 2008].

146
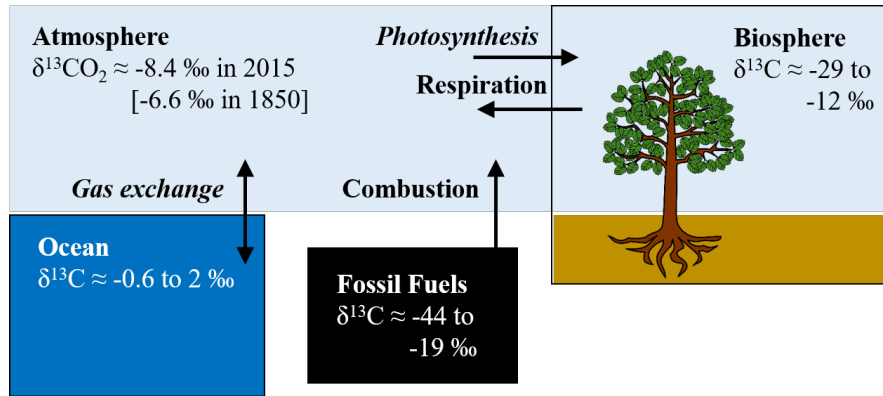
147

148　Figure 1. Diagram of ^{13}C in the global carbon cycle showing the pools interacting with
149　atmospheric CO_2 on the timescale of the Industrial Period. Typical ranges of δ^{13}C are shown for
150　each of the pools [*Andres et al.*, 2000; *Bowling et al.*, 2008; *Graven et al.*, 2017; *Olsen et al.*,
151　2016]. Global average $\delta^{13}CO_2$ was -8.4 ‰ in 2015 and -6.6 ‰ in 1850. Processes involving
152　significant fractionation are shown in italics, processes without significant fractionation are
153　shown in normal text.

154

3. The Nuclear Bomb Effect for ^{14}C

155

156　In the 1950s and 1960s, nuclear weapons testing produced ^{14}C in the atmosphere, strongly
157　enriching ^{14}C and counteracting the Suess Effect. This effect was termed the "Atom Bomb
158　Effect" when first reported by *Rafter and Fergusson* [1957]; we refer to it as the "Nuclear Bomb
159　Effect". The process for ^{14}C production was similar to the natural production of ^{14}C in the
160　atmosphere: neutrons produced by the hydrogen bomb explosions react with atmospheric
161　nitrogen to produce ^{14}C. Most of the nuclear explosions and ^{14}C production took place in the
162　Northern Hemisphere, and most tests and particularly the largest tests occurred shortly before the
163　Partial Test Ban Treaty came into effect in 1963 [*Naegler and Levin*, 2006].

164　There is an ongoing production of ^{14}C by the nuclear industry at nuclear power plants, with the
165　^{14}C production varying by type of reactor. The amount of ^{14}C produced by the nuclear industry
166　and released to the atmosphere is only about 10% of the natural production of ^{14}C [*Graven and
167　Gruber*, 2011] so the effects on $\Delta^{14}CO_2$ are much smaller than the effects from the nuclear
168　weapons testing, which, in contrast, exceeded the rate of natural production by 2 orders of
169　magnitude [*Naegler and Levin*, 2006]. Nuclear power plant emissions ramped up between the
170　1970s and 1990s as the nuclear industry expanded, but they appear to have recently started to fall
171　[*Zazzeri et al.*, 2018].

172

4. Natural Carbon Cycle Response to the Suess and Nuclear Bomb Effects

173

174　By perturbing the isotopic composition of atmospheric CO_2, the Suess and Nuclear Bomb Effects
175　have also affected all the other carbon reservoirs in the ocean and on land that exchange with
176　atmospheric CO_2 on decadal to centennial timescales (Figures 1 and 2). These exchanges
177　between the atmosphere and other carbon reservoirs have modulated the changes to atmospheric
178　CO_2, effectively mixing the anthropogenic emissions into a larger carbon pool that encompasses
179　atmospheric CO_2 and land and ocean carbon with residence times of about a century or less.

180
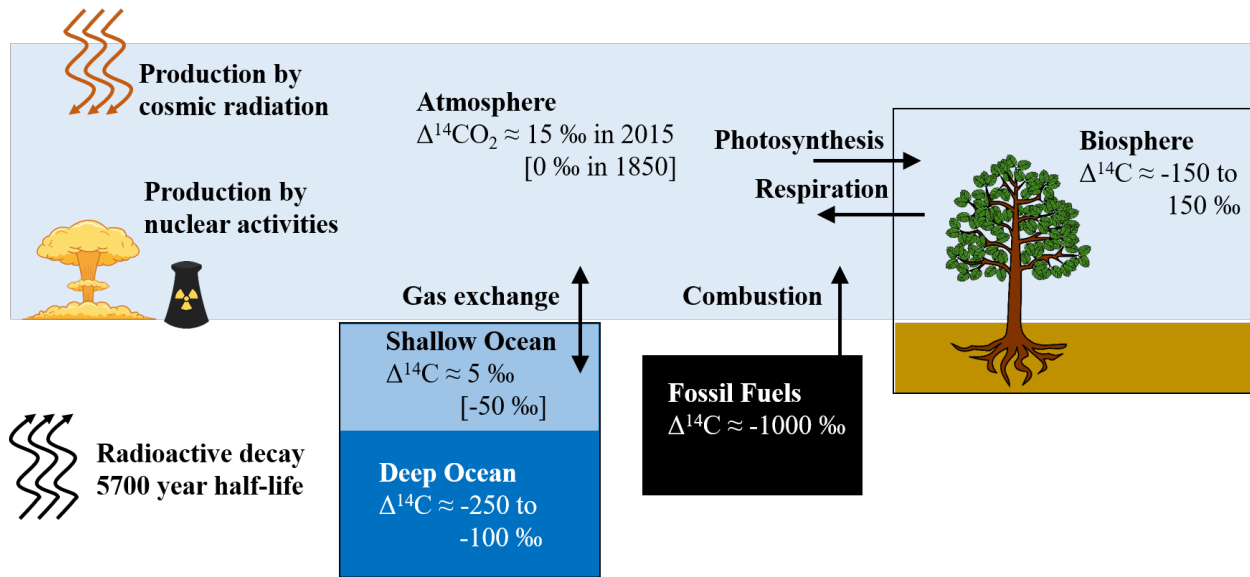
181
182 Figure 2. Diagram of ^{14}C in the global carbon cycle showing the pools interacting with
183 atmospheric CO_2 on the timescale of the Industrial Period. Typical ranges of $\Delta^{14}C$ are shown for
184 each of the pools. Global average $\Delta^{14}CO_2$ was approximately 15 ‰ in 2018 and 0 ‰ in 1850,
185 whereas $\Delta^{14}CO_2$ in the troposphere was much higher in 1964-65, 600 to 1000 ‰ (Figure 3). In
186 the shallow ocean, average $\Delta^{14}C$ was approximately 5 ‰ in 2018 and -50 ‰ in 1850. Production
187 of ^{14}C occurs naturally through cosmic radiation, and anthropogenically through nuclear
188 activities. All ^{14}C undergoes radioactive decay with a half-life of 5700 years.

189

190 On land, the CO_2 taken up by photosynthesis carries the stable isotopic signature of atmospheric
191 CO_2, modified by fractionation during photosynthesis (Figure 1). Photosynthetic fractionation,
192 also called discrimination, varies by plant type. Most trees are C_3 plants that discriminate more
193 than C_4 plants like grasses, with the $\delta^{13}C$ of the fixed carbon approximately 18 ‰ lower in C_3
194 and 4 ‰ lower in C_4 plants than in atmospheric CO_2. The CO_2 returned to the atmosphere by
195 respiration carries the isotopic signature of the organic material being respired, which can have a
196 range of ages. Fractionation does not occur during respiration [*Lin and Ehleringer*, 1997],
197 although there can be differences in $\delta^{13}C$ between different plant and soil compounds or
198 gradients within plants that can lead to variation in $\delta^{13}C$ of respiration [*Bowling et al.*, 2008].

199 Similarly, the CO_2 entering the ocean through air-sea exchange carries the stable isotopic
200 signature of atmospheric CO_2, modified by fractionation during gas transfer (Figure 2). The CO_2
201 exiting the ocean carries the isotopic signature of dissolved inorganic carbon (DIC) at the
202 surface, modified by fractionation during gas transfer. Fractionation during gas transfer includes
203 both kinetic and equilibrium effects [*Zhang et al.*, 1995] and results in ocean DIC being ^{13}C-
204 enriched compared to atmospheric $\delta^{13}CO_2$. The $\delta^{13}C$ of ocean waters are also influenced by
205 marine ecosystems such that the net photosynthesis in the surface ocean and net respiration at
206 depth cause $\delta^{13}C$ to generally decrease with depth [*Eide et al.*, 2017].

207 The gross fluxes to the atmosphere from the terrestrial biosphere and the ocean, and vice versa,
208 also carry the radiocarbon signature of the respective pool. Because of the fractionation
209 correction used in the $\Delta^{14}C$ notation, the processes involving fractionation do not alter the $\Delta^{14}C$

210   signature of the carbon leaving one pool and entering another. Differences in the Δ^{14}C signature
211   of different pools are caused by natural or anthropogenic ^{14}C production and by radioactive
212   decay. Before the Suess and Nuclear Bomb effects, Δ^{14}C in terrestrial and oceanic pools was
213   lower than atmospheric Δ^{14}C because of radioactive decay, depending on how long the carbon
214   was isolated from the atmosphere. The Δ^{14}C in new leaves would be nearly the same as
215   atmospheric Δ^{14}C, whereas the Δ^{14}C in the deep ocean or in aged soils would be much lower.

216   The decline in atmospheric $\delta^{13}CO_2$ since the Industrial Revolution has resulted in the CO_2 taken
217   up by photosynthesis being lighter than CO_2 returned to the atmosphere by respiration. Similarly,
218   the CO_2 taken up by the ocean is lighter than the CO_2 returned to the atmosphere. Therefore, the
219   net land exchange and net ocean exchange are causing a net flux of ^{13}C from the terrestrial
220   biosphere to the atmosphere and from the ocean to the atmosphere that partly counteracts the
221   decline in atmospheric $\delta^{13}CO_2$. These are referred to as "disequilibrium fluxes." In addition, the
222   discrimination against ^{13}C that occurs during photosynthesis may be increasing over time
223   [*Keeling et al.*, 2017; *Schubert and Jahren*, 2012], causing even less ^{13}C to be removed by
224   photosynthesis. Discrimination is increasing because of the impact of rising atmospheric CO_2
225   concentration on photorespiration and mesophyll processes. Individual plants and ecosystems
226   may have also experienced changes in δ^{13}C due to variation or trends in climate that influence
227   the strength of ^{13}C discrimination. Air-sea exchange of ^{13}C is also influenced by ocean
228   temperature, wind speed and biological productivity. Changes in these properties may have also
229   caused small influences on the atmospheric $\delta^{13}CO_2$ trend over the Industrial Period [*Keeling et
230   al.*, 2017].

231   The Suess Effect has a similar effect on ^{14}C, such that decreases in atmospheric $\Delta^{14}CO_2$ lead to
232   net effluxes of ^{14}C from the land biosphere and the ocean that partly counteract the decrease in
233   atmospheric $\Delta^{14}CO_2$ [*Stuiver and Quay*, 1981]. The nuclear weapons tests had the opposite
234   effect. The Nuclear Bomb Effect caused the atmosphere to become highly enriched in ^{14}C and
235   land and ocean exchanges acted to remove ^{14}C and decrease $\Delta^{14}CO_2$ [*Levin and Hesshaimer*,
236   2000]. Now that several decades have passed since the bomb testing ended, the land and ocean
237   exchanges of ^{14}C have become more complex. There are both positive and negative influences
238   on $\Delta^{14}CO_2$. Reservoirs where the carbon is stored for a matter of years quickly became more
239   enriched in ^{14}C following the atmosphere, but with a lag. Now, as atmospheric Δ^{14}C is falling,
240   the Δ^{14}C of these reservoirs is again falling behind the atmosphere trend. These reservoirs,
241   which include carbon in terrestrial vegetation and in the surface waters of subtropical ocean
242   gyres, are now positive influences on $\Delta^{14}CO_2$, releasing ^{14}C back to the air [*Graven et al.*, 2012c;
243   *Randerson et al.*, 2002a]. Reservoirs that exchange with the atmosphere on longer timescales,
244   such as the carbon in the surface water of the Southern Ocean, remain lower in Δ^{14}C and
245   continue to be a negative influence on $\Delta^{14}CO_2$ today [*Graven et al.*, 2012c].

246   In the simple diagrams in Figures 1 and 2, and in the simple carbon cycle model we present later,
247   we have omitted the conduit of terrestrial carbon to the ocean via rivers, which comprises 0.4 to
248   0.8 PgC/yr [*Resplandy et al.*, 2018]. The impacts of rivers on atmospheric $\delta^{13}CO_2$ and $\Delta^{14}CO_2$
249   are likely to be small overall, since the riverine flux is much smaller than the gross fluxes
250   between atmospheric CO_2 and the terrestrial biosphere and ocean, but the carbon in rivers will
251   respond to atmospheric $\delta^{13}CO_2$ and $\Delta^{14}CO_2$ and changing environmental conditions that affect
252   terrestrial and riverine carbon cycling. Radiocarbon measurements have revealed differences in
253   the age of dissolved and particulate organic carbon in rivers that help to identify the source
254   [*Marwick et al.*, 2015]. There is also evidence that land use has altered the age of the terrestrial

255 carbon exported to the ocean, where deforestation increases the transport of aged soil organic
256 carbon in rivers and its subsequent remineralization [*Drake et al.*, 2019].

257

5. Atmospheric Changes over the Industrial Period

259 The changes in atmospheric $\delta^{13}CO_2$ and $\Delta^{14}CO_2$ over the Industrial Period have been quantified
260 using a combination of direct sampling of the atmosphere and records of atmospheric
261 composition from tree rings, ice cores and firn. Regular observations of $\delta^{13}CO_2$ and $\Delta^{14}CO_2$ have
262 been made by direct measurements of air samples since the 1970s for $\delta^{13}CO_2$ [*Allison and*
263 *Francey*, 2007; *Keeling et al.*, 2005; *Vaughn et al.*, 2010], and the 1950s for $\Delta^{14}CO_2$ [*Levin et al.*,
264 2010; *Turnbull et al.*, 2016]. Records of $\delta^{13}CO_2$ and $\Delta^{14}CO_2$ prior to direct measurements have
265 been constructed using measurements of air in ice cores and firn for $\delta^{13}CO_2$ [*Rubino et al.*, 2013]
266 and tree ring cellulose and other materials for $\Delta^{14}CO_2$ [*Hogg et al.*, 2013; *Reimer et al.*, 2013].

267 Recently, various records have been compiled and harmonized to provide a consistent record of
268 global $\delta^{13}CO_2$ and $\Delta^{14}CO_2$ changes over the Industrial Period, 1850-2015 [*Graven et al.*, 2017]
269 (Figure 3). These compiled records provide annual averages for global $\delta^{13}CO_2$ and for $\Delta^{14}CO_2$ in
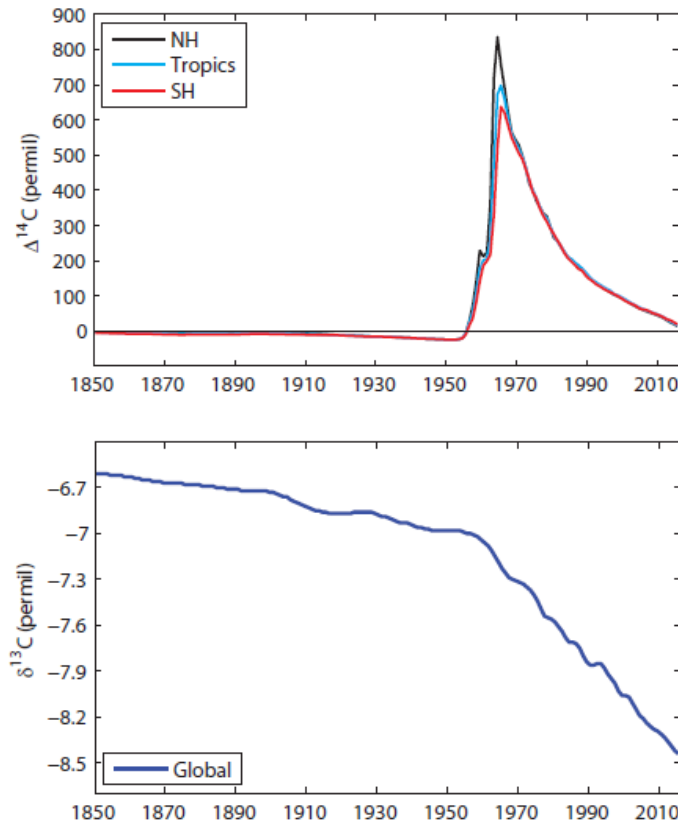270 three zonal bands.

271 From 1850 to 2015 atmospheric $\delta^{13}CO_2$ decreased by 1.8 ‰, with 1.5% of this drop occurring
272 since 1950 (Figure 3) [*Graven et al.*, 2017; *Rubino et al.*, 2013]. The *Graven et al.* [2017]
273 compilation shows a smaller change in $\delta^{13}CO_2$ over the Industrial Period, 1850 to 2015, than in
274 previous estimates. Measurements of $\delta^{13}CO_2$ reported by *Bauska et al.* [2015] and *Friedli et al.*
275 [1986] between 1850 and 1950 are approximately 0.05 ‰ and 0.12 ‰ higher, respectively, than
276 in *Graven et al.* [2017] so that when combined with recent flask data the change since 1850
277 appears larger. The difference arises from the methods of to convert calcite ^{13}C standards into
278 CO_2 and implement the VPDB scale at individual laboratories [*Brand et al.*, 2009]. Laboratory
279 offsets can be larger than 0.1 ‰, much larger than the compatibility goal of ±0.01 ‰
280 [*WMO/IAEA*, 2003; 2018]. We expect the data reported by *Graven et al.* [2017] to be the most
281 robust estimate available of the $\delta^{13}CO_2$ change since 1850 because they ensured that the data
282 from both periods was from the same laboratory (CSIRO), while also incorporating recent flask
283 data from other laboratories by quantifying laboratory offsets. Ongoing activities to distribute
284 reference materials of pure CO_2 or CO_2 in whole air show promise for improving measurement
285 compatibility [*Wendeberg et al.*, 2013; *WMO/IAEA*, 2018]

286 Atmospheric $\Delta^{14}CO_2$ decreased by approximately 20 ‰ between 1850 and 1950 as a result of
287 fossil fuel emissions after the Industrial Revolution [*Suess*, 1955] (Figure 3). Then $\Delta^{14}CO_2$ rose
288 rapidly from the mid-1950s until the mid-1960s during the period of intense nuclear weapons
289 testing [*Rafter and Fergusson*, 1957]. Tropospheric $\Delta^{14}CO_2$ reached its highest level in 1964-65,
290 which was 835 ‰ in the Northern Hemisphere annual average (Figure 3). After the peak in
291 1964-65, $\Delta^{14}CO_2$ decreased at a nearly exponential rate as the "bomb ^{14}C" mixed into the ocean
292 and terrestrial biosphere. Initially, large gradients were observed between the Northern and
293 Southern Hemispheres because most of the bomb tests occurred in the Northern Hemisphere
294 (Figure 3) [*Nydal and Lövseth*, 1983]. The large interhemispheric gradients in the atmosphere
295 weakened after a few years through atmospheric mixing. Since the 1990s the decrease of $\Delta^{14}CO_2$
296 has been almost linear at about 5 ‰ yr^{-1}, now driven primarily by fossil fuel emissions [*Graven*
297 *et al.*, 2012b; *Levin et al.*, 2010]. The interhemispheric gradient has switched sign: now $\Delta^{14}CO_2$
298 in the Northern Hemisphere is about 5 ‰ lower than in the Southern Hemisphere. Both the

299    $\Delta^{14}CO_2$ trend and the interhemispheric gradient are weaker than expected from fossil fuel
300   emissions alone because of the combined influence on $\Delta^{14}CO_2$ from carbon exchanges with the
301   ocean and land biosphere, and by natural ^{14}C production and ^{14}C emissions from nuclear power
302   plants.

303

304

305   Figure 3: Compiled historical datasets for $\Delta^{14}CO_2$ (top) and $\delta^{13}CO_2$ (bottom) from *Graven et al.*
306   [2017]. Annual mean values of $\Delta^{14}C$ are provided for three zonal bands representing the
307   Northern Hemisphere (30°N-90°N), the Tropics (30°S-30°N) and the Southern Hemisphere
308   (30°S-90°S). Annual mean, global mean values are provided for $\delta^{13}C$.

309

310   How would atmospheric $\Delta^{14}CO_2$ have evolved in response to the Suess Effect, if there had been
311   no bomb tests? And how would the Nuclear Bomb Effect have evolved in the absence of fossil
312   fuel emissions? To demonstrate the different effects of fossil fuel emissions and nuclear weapons
313   testing on $\Delta^{14}CO_2$, we conducted simulations with a simple carbon cycle model under two
314   hypothetical scenarios. One is a scenario with nuclear weapons testing, but without fossil fuel
315   emissions. The other scenario includes fossil fuel emissions, but no nuclear weapons testing.
316   Details of the simulations are given in SM1.

317   Under the scenario without fossil fuel emissions, global atmospheric $\Delta^{14}CO_2$ peaks at a higher
318   level of 790 ‰ (compared to the observed value in the tropics in 1965 of approximately 700 ‰)
319   because, in this case, the bomb-derived ^{14}C is mixed into a lower concentration of atmospheric
320   CO_2. After the peak in $\Delta^{14}CO_2$, it exponentially declines in a similar way to that observed until

321   around 1990. Then, the simulated $\Delta^{14}CO_2$ decline slows, whereas the observed $\Delta^{14}CO_2$ decline
322   continues at a nearly steady rate after 1990. This divergence of the simulated and observed
323    $\Delta^{14}CO_2$ shows how the importance of the Suess Effect has strengthened in the past few
324   decades[*Graven et al.*, 2012b; *Levin et al.*, 2010]. Without fossil fuel emissions, $\Delta^{14}CO_2$ would
325   have been about 150 ‰ higher than observed in 2015.

326   Under the scenario without nuclear weapons testing, atmospheric $\Delta^{14}CO_2$ decreases throughout
327   the period 1850 to 2015, reaching -130 ‰ in 2015. Without the addition of ^{14}C from the weapons
328   tests, the Suess Effect would have reduced $\Delta^{14}CO_2$ substantially below preindustrial levels by
329   now.

330
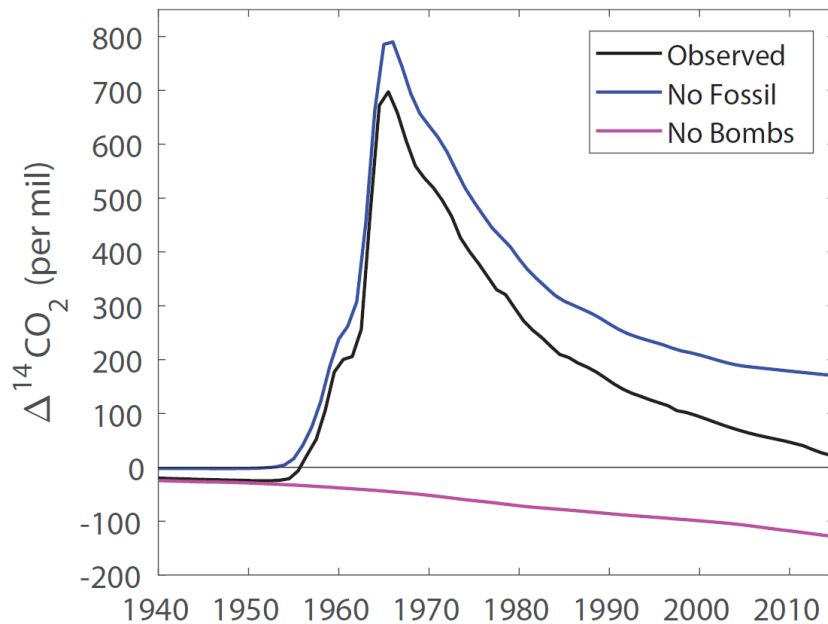
331

332   Figure 4: Observed $\Delta^{14}CO_2$ and simulated $\Delta^{14}CO_2$ for scenarios without nuclear weapons tests
333   ("No Bombs") or without fossil fuel burning ("No Fossil").

334

335   **6. Applications of Atmospheric $^{13}CO_2$ Measurements**

336   Observations of atmospheric $\delta^{13}CO_2$ have been used in many applications to investigate carbon
337   fluxes and the functioning of plants. A major application has been the so-called "double
338   deconvolution" on historical CO_2 and $\delta^{13}CO_2$ data to partition CO_2 uptake by the ocean vs the
339   terrestrial biosphere [*Keeling et al.*, 1989]. These studies use mass balance equations and model
340   simulations that account for fractionation and changing disequilibrium fluxes. The double
341   deconvolution method has been used with direct atmospheric measurements to attribute
342   interannual variations in CO_2 growth rate to land and ocean sources, concluding that El Niño
343   events are associated with an anomalous terrestrial source of CO_2 [*Keeling et al.*, 1995]. The
344   double deconvolution method has also been used with ice core and firn data to investigate
345   centennial- to millennial-scale variations associated with climate variability, indicating the
346   terrestrial response to temperature is generally stronger than the ocean's response [*Trudinger et*
347   *al.*, 1999]. The double deconvolution suggested that the low CO_2 growth rate in the 1940s was

348   driven by the ocean [*Trudinger et al.*, 2002], although this conclusion remains controversial
349   [*Bastos et al.*, 2016; *Rafelski et al.*, 2009].

350   Atmospheric inversions have been used to estimate spatially-resolved fluxes of carbon and ^{13}C
351   based on atmospheric data and models. These operate similarly to the double deconvolution. The
352   first study employed a two-dimensional atmospheric model and helped to identify the "missing
353   sink" of carbon in the land biosphere and particularly in the Northern Hemisphere [*Ciais et al.*,
354   1995]. Subsequent three-dimensional studies indicated that land and ocean CO_2 sinks were
355   comparable in magnitude, and that CO_2 uptake increased in the Northern Hemisphere after the
356   Pinatubo eruption in 1991, in addition to the interannual variability related to El Niño [*Enting et*
357   *al.*, 1995; *Rayner et al.*, 1999]. A shortcoming of these studies was that variability in plant ^{13}C
358   discrimination was not considered. In reality, plant ^{13}C discrimination and CO_2 uptake are
359   expected to be correlated, for example, because drought will reduce both productivity and
360   discrimination as plants close their stomata to minimize water loss [*Randerson et al.*, 2002b].
361   Expanding the methodology to estimate discrimination as part of the inversion, *Peters et al.*
362   [2018] estimated variations in water use efficiency on continental scales and showed that global
363   models underestimated the drought response of plants.

364   The potential for long term trends in plant discrimination had also been neglected in global
365   studies using the double deconvolution. Using historical $\delta^{13}CO_2$ data with a simple carbon cycle
366   model, *Keeling et al.* [2017] found that ^{13}C discrimination is likely to have strengthened by 0.7
367   ‰ between 1975 and 2005, which is consistent with a dependence on CO_2 concentration that has
368   been found in laboratory and paleo studies and attributed to mesophyll and photorespiration
369   effects [*Schubert and Jahren*, 2012]. *Keeling et al.* [2017] further argue that the past double
370   deconvolution studies have neglected a mechanistic link between land and ocean isotopic fluxes
371   that means long-term $\delta^{13}CO_2$ data actually do not provide a strong constraint on land and ocean
372   CO_2 sinks. For example, changing the ocean diffusivity in a simple model changes the ocean
373   CO_2 uptake and ^{13}C flux, but it creates compensating changes in the ^{13}C flux to the land via the
374   residual CO_2 flux needed to maintain mass balance. Therefore, ocean diffusivity (which governs
375   ocean CO_2 uptake) does not have a strong influence on the long-term $\delta^{13}CO_2$ trend.

376   Atmospheric $\delta^{13}CO_2$ measurements are commonly used to investigate terrestrial biosphere
377   activity on local or regional scales by estimating isotopic signatures of photosynthesis or
378   respiration using the "Keeling Plot" approach. The "Keeling Plot" [*Keeling*, 1958], or alternative
379   formulations such as the "Miller-Tans Plot" [*Miller and Tans*, 2003], quantifies the isotopic
380   signature of a CO_2 source or sink by manipulating the CO_2 and $^{13}CO_2$ mass balance equations so
381   that the isotopic signature is given by the intercept or slope of a regression fit. These studies have
382   revealed a strong link between isotopic fluxes and water availability [*Pataki et al.*, 2003]. They
383   have helped to explain the driving factors of water use efficiency by plants, a metric for the
384   amount of productivity per unit water loss, and how these factors affect spatial and temporal
385   patterns of water use efficiency [*Bowling et al.*, 2002]. These studies typically sample air in
386   flasks that are subsequently analyzed for $\delta^{13}CO_2$ by mass spectrometry in the laboratory, but now
387   optical instruments that measure $^{13}CO_2$ are increasingly used in the field. These instruments have
388   also enabled eddy covariance measurements of $^{13}CO_2$ fluxes, uncovering the suppression of
389   daytime respiration [*Wehr et al.*, 2016].

390   Other studies have measured $\delta^{13}CO_2$ in urban areas to investigate fossil fuel emissions. In
391   combination with other tracers such as $\Delta^{14}CO_2$ or $\delta^{18}O$ of CO_2, $\delta^{13}CO_2$ measurements have been

392   useful for determining the proportion of natural gas vs petroleum contributions to fossil fuel CO_2
393   emissions in urban areas [*Newman et al.*, 2016; *Pataki et al.*, 2007].

394   Measurements of atmospheric $\delta^{13}CO_2$ are also critical to other studies that do not interpret the
395   measurements directly but rather use them for comparison with $\delta^{13}C$ measured in other materials.
396   In terrestrial ecology, atmospheric $\delta^{13}CO_2$ is compared to $\delta^{13}C$ in tree rings or leaves to
397   investigate spatial patterns and temporal variation in the internal leaf CO_2 concentration and
398   thereby, the response of plant productivity to climate, atmospheric CO_2 and other variables
399   [*Frank et al.*, 2015; *Wang et al.*, 2017]. Measurements of $\delta^{13}C$ in dissolved inorganic carbon in
400   the ocean have been compared with atmospheric $\delta^{13}CO_2$ to estimate anthropogenic CO_2 uptake
401   [*Gruber and Keeling*, 2001; *Quay et al.*, 2003]. Comparisons with atmospheric $\delta^{13}CO_2$ are also
402   used in ecological studies of the diet, trophic structure, physiology and local environment of
403   animals [*DeNiro and Epstein*, 1978].

404

405   7. Applications of Atmospheric $^{14}CO_2$ Measurements

406   Observations of atmospheric $\Delta^{14}CO_2$ have been used in many applications to investigate the
407   global carbon cycle [*Levin and Hesshaimer*, 2000]. *Suess* [1955]'s measurement of industrial-era
408    $\Delta^{14}CO_2$ via tree ring records comprised some of the first evidence of the strong impact of fossil
409   fuel burning on atmospheric CO_2, predating the start of C.D. Keeling's long-term CO_2
410   concentration measurements [*Keeling*, 1960]. The first direct measurements of atmospheric
411    $\Delta^{14}CO_2$ were made around the same time as the nuclear weapons tests, revealing large spatial
412   gradients caused by the location of the nuclear tests. These observations were used to investigate
413   atmospheric mixing and showed that the interhemispheric exchange time in the troposphere is
414   about one year, and the mixing between the stratosphere and troposphere has a seasonal variation
415   [*Lal and Rama*, 1966; *Nydal*, 1966].

416   Other studies have investigated ocean or terrestrial biosphere CO_2 fluxes using $\Delta^{14}CO_2$
417   measurements. By using $\Delta^{14}CO_2$ measurements and carbon cycle models to construct an
418   inventory of bomb-derived ^{14}C in each of the main carbon reservoirs, *Hesshaimer et al.* [1994]
419   showed that previous estimates of the ocean ^{14}C inventory [*Broecker et al.*, 1985] had been too
420   high. This implied that the depth to which bomb-derived ^{14}C had penetrated into the ocean and
421   the amount of CO_2 that had been taken up were also overestimated. Several other studies have
422   used oceanic measurements of $\Delta^{14}C$ in dissolved inorganic carbon to estimate the air-sea gas
423   exchange velocity [*Naegler et al.*, 2006; *Sweeney et al.*, 2007; *Wanninkhof*, 2014]. Changes in
424   ocean circulation that impact the air-sea exchange of ^{14}C have been inferred from $\Delta^{14}CO_2$
425   measured on timescales of interannual, El Niño events [*Rozanski et al.*, 1995] and timescales of
426   decades to centuries [*Rodgers et al.*, 2011]. The magnitude of net primary production in the
427   terrestrial biosphere has also been estimated [*Naegler and Levin*, 2009] using $\Delta^{14}CO_2$
428   measurements and carbon cycle models to construct an inventory of bomb-derived ^{14}C, in a
429   similar approach to *Hesshaimer et al.* [1994]. A few studies have also considered the effect of
430   biospheric carbon fluxes on atmospheric $\Delta^{14}CO_2$ measurements. Signatures of elevated $\Delta^{14}C$ in
431   respiration were postulated for seasonal cycles of $\Delta^{14}CO_2$ in North America [*LaFranchi et al.*,
432   2016] and for the large scale meridional gradients of $\Delta^{14}CO_2$ [*Levin and Hesshaimer*, 2000].

433   A major and growing application for atmospheric $\Delta^{14}CO_2$ measurements is the calculation of
434   local CO_2 added by fossil fuel combustion (ffCO_2). Evidence for a regional Suess Effect had
435   already appeared in comparisons of tree ring data [*Tans et al.*, 1979]. Then, I. Levin developed

436   the methodology for the calculation of $ffCO_2$ with atmospheric observations in Europe in the
437   1980s [*Levin et al.*, 1989]. The method attributes regional gradients in $\Delta^{14}CO_2$ to fossil fuel
438   emissions, while accounting for other regional influences on $\Delta^{14}CO_2$ from heterotrophic
439   respiration and nuclear power plants (β) [*Turnbull et al.*, 2006]:

440
$$ffCO_2 = C_m \frac{\Delta bg - \Delta m}{\Delta bg + 1000‰} + \beta \qquad (1)$$

441   Here C_m is the measured CO_2 concentration, Δm is the measured $\Delta^{14}CO_2$ and Δbg is the $\Delta^{14}CO_2$
442   at a "background" site that is upwind of the region of interest. β represents a correction for non-
443   fossil fuel influences on $\Delta^{14}CO_2$, which could include heterotrophic respiration or ^{14}C emissions
444   from nuclear power plants. I. Levin and colleagues have measured $\Delta^{14}CO_2$ in the city of
445   Heidelberg since 1986, comparing it to measurements from Jungfraujoch in the Swiss Alps to
446   calculate $ffCO_2$ [*Levin et al.*, 2003; *Levin et al.*, 2011]. Their measurements have shown little
447   change in the $ffCO_2$ present in Heidelberg, similar to reported trends in local emissions.
448   Observing system simulation experiments have demonstrated that $\Delta^{14}CO_2$ measurements have a
449   strong potential for improving atmospheric observation-based estimates of not only regional
450   fossil fuel emissions but also biospheric fluxes [*Basu et al.*, 2016; *Fischer et al.*, 2017]. In the
451   state of California, USA, measurements of $\Delta^{14}CO_2$ from a network of towers were combined
452   with a regional atmospheric transport model in an atmospheric inversion to estimate fossil fuel
453   emissions, finding that reported emissions were consistent with $\Delta^{14}CO_2$ observations [*Graven et
454   al.*, 2018]. In an atmospheric inversion applied to $\Delta^{14}CO_2$ measurements across North America,
455   estimated emissions for the entire USA were consistent with those officially reported but
456   significantly higher than some other commonly used fossil fuel emissions data products [*Basu et
457   al.*, 2020]. Some other studies have combined $\Delta^{14}CO_2$ measurements with CO, a combustion
458   product that can be measured continuously [*Turnbull et al.*, 2015; *Vogel et al.*, 2010]. However,
459   other than the measurements from Heidelberg and some regional campaigns, the method has yet
460   to be systematically implemented for the evaluation of regional $ffCO_2$ emissions.

461   Applications making use of $\Delta^{14}CO_2$ measurements for comparison with $\Delta^{14}C$ in other materials
462   are much more numerous than for $\delta^{13}CO_2$, and they span a broad range of fields including
463   archaeology, physiology and forensics [*Bronk Ramsey*, 2008; *Geyh*, 2001; *Spalding et al.*, 2005].
464   Within carbon cycle science, $\Delta^{14}C$ measurements are widely used in ecology and soil science to
465   determine the residence time of carbon in different compound classes [*Trumbore*, 2000].

466   Some applications combine $\delta^{13}C$ and $\Delta^{14}C$ to draw more powerful inferences from the
467   combination that was possible with either alone. For example, *Keeling et al.* [2017] showed that
468   atmospheric $\delta^{13}CO_2$ trends could not be matched by a carbon cycle model constrained by
469   radiocarbon data, unless changes in ^{13}C discrimination during photosynthesis were included in
470   the model. *Krakauer et al.* [2006] analyzed spatial patterns in both atmospheric $\Delta^{14}CO_2$ and
471    $\delta^{13}CO_2$ to investigate the air-sea gas exchange velocity.

472

473   **8. Projected Future Changes in $\delta^{13}CO_2$ and $\Delta^{14}CO_2$**

474   In the future, atmospheric $\delta^{13}CO_2$ and $\Delta^{14}CO_2$ will continue to evolve in response to the fossil
475   fuel emissions and other human activities, and the carbon cycle responses to them. Future
476   simulations of $\Delta^{14}CO_2$ were first presented by *Caldeira et al.* [1998] for the IS92a "business-as-
477   usual" emission scenario from the 1st IPCC Assessment Report. They showed that increasing
478   fossil fuel emissions cause $\Delta^{14}CO_2$ to decrease to lower than -150 ‰ in 2100. While $\Delta^{14}CO_2$

479 decreases strongly, the number of atoms of ^{14}C in the atmosphere actually increases due to a
480 large efflux of ^{14}C from the ocean to the atmosphere in response to the changing air-sea
481 disequilibrium. *Graven* [2015] ran similar simulations using the Representative Concentration
482 Pathways from the 5th IPCC Report considering not just business-as-usual but a range of future
483 scenarios [*Meinshausen et al.*, 2011]. She found a range of possible paths for $\Delta^{14}CO_2$ through
484 this century, with the high fossil fuel emission scenario dropping to less than -230 ‰ in 2100 but
485 a mitigation scenario in line with limiting global warming below 2°C dropping to about -20 ‰ in
486 the 2030s and then remaining nearly steady. She made important inferences about the impacts of
487 these different scenarios. The high fossil fuel emission scenario creates ambiguity in the use of
488 radiocarbon dating because at some point during the century "new" materials would have the
489 same radiocarbon age as materials that are up to two thousand years old, with impacts on
490 archaeology and forgery detection. In contrast, scenarios where $\Delta^{14}CO_2$ stops decreasing imply
491 that applications in ecology, forensics and physiology that make use of the $\Delta^{14}CO_2$ trend as a
492 shorter-term clock would no longer be viable.

493 The first simulations of future $\delta^{13}CO_2$ were presented by *Köhler* [2016] using the Representative
494 Concentration Pathways. They showed continued declines in $\delta^{13}CO_2$ as fossil fuel emissions
495 grow in high emission scenarios, but reversals of $\delta^{13}CO_2$ trends for low emission scenarios.
496 There was a range of about 5 ‰ between the high fossil fuel emission and mitigation scenarios
497 in 2100, with the most stringent mitigation scenario reaching a minimum around mid-century
498 and then increasing by several per mil.

499 The future scenarios being considered for the 6th IPCC Report by the Coupled Model
500 Intercomparison Project (CMIP) are now based on a set of five narratives, called the Shared
501 Socioeconomic Pathways (SSPs) [*O'Neill et al.*, 2014]. Scenarios ranging from worlds without
502 climate action to very stringent mitigation scenarios in line with limiting global warming to
503 1.5°C have been explored for each of these narratives [*Riahi et al.*, 2017; *Rogelj et al.*, 2018].
504 Finally, a selection of SSP-based scenarios have been identified as the main scenarios to be
505 examined in CMIP6 [*O'Neill et al.*, 2016]. The atmospheric CO_2 concentration, fossil fuel
506 emissions and land use emissions for six of the key SSP-based scenarios are shown in Fig 5
507 [*Hoesly et al.*, 2018; *Meinshausen et al.*, 2017]. These pathways employ varying amounts of
508 "negative emissions" from deliberate CO_2 removal and the net fossil fuel emissions including
509 negative emissions are also shown in Fig 5. These SSP-based scenarios span a larger range of
510 possible future pathways than the RCPs, including a lower emission pathway consistent with a
511 maximum end-of-century warming of 1.5°C (SSP1-1.9) as well as a very high emission pathway
512 without controls on greenhouse gas emissions (SSP5-8.5). There is also an "overshoot" scenario
513 where atmospheric CO_2 concentration rises until mid-century and then decreases rapidly as a
514 result of strong and targeted CO_2 removal activities (SSP5-3.4os). The process for deliberate
515 CO_2 removal included in the SSP scenarios is Bioenergy with Carbon Capture and Storage
516 (BECCS). In this way, the CO_2 removal is mediated by an initial uptake into the terrestrial
517 biosphere, which has implications for atmospheric $\delta^{13}CO_2$ [*Köhler*, 2016]. BECCS acts like an
518 "anti-Suess Effect", enriching atmospheric $\delta^{13}CO_2$ by preferentially removing ^{12}C through
519 photosynthesis and burial of biofuel-derived CO_2.

520 Our simulations of future atmospheric $\delta^{13}CO_2$ and $\Delta^{14}CO_2$ consider the change in atmospheric
521 CO_2 concentration, fossil fuel emissions, land use emissions and BECCS, as well as the response
522 of the carbon cycle to these changes (Figure 5). In addition, future changes in ^{13}C discrimination
523 by land plants are included as a function of atmospheric CO_2 concentration following *Schubert*

524 *and Jahren* [2015], and changes in air-sea fractionation factors are included as a function of sea
525 surface temperature and dissolved carbonate concentration [*Orr et al.*, 2017]. Future changes to
526 the $\delta^{13}C$ in fossil fuel emissions were not included because there was not enough information
527 provided with the SSP-based scenarios to estimate them. Further details of the future simulations
528 are given in SM2.

529

530
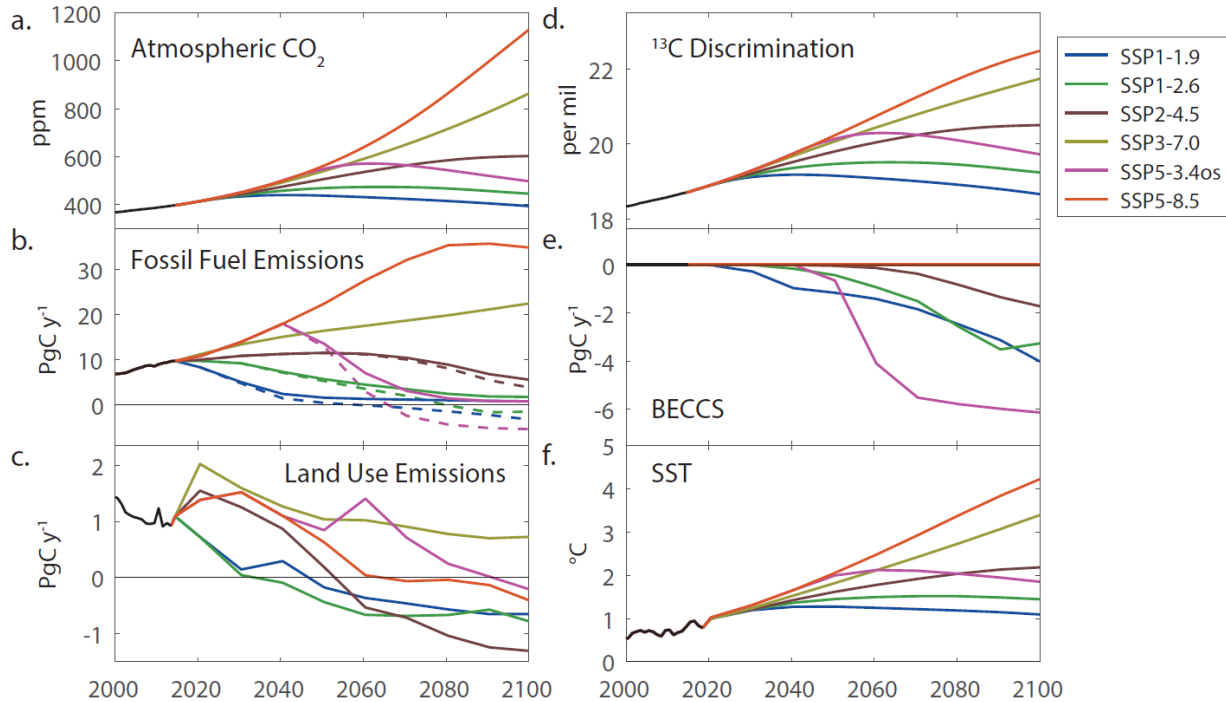
Figure 5: (a) Atmospheric CO₂, (b) fossil fuel emissions, (c) land use emissions, (d) ^{13}C
discrimination, (e) CO₂ removal by BECCS and (f) global mean sea surface temperature (SST)
used in the future simulations. In (b) the gross fossil fuel emissions are shown with solid lines
while dashed lines show net emissions accounting for BECCS. Historical data are shown in
black until 2015, then the six SSP-based scenario projections are shown for 2015-2100.

536

537 The simulations show that atmospheric $\Delta^{14}CO_2$ drops below 0 ‰ within the next few years in all
538 scenarios (Fig. 6). In the lowest emission scenario, SSP1-1.9, where net fossil fuel emissions
539 reach zero around 2050 (Fig. 5), $\Delta^{14}CO_2$ stays around 0 ‰ for about ten years and then increases
540 again, remaining at about 10-12 ‰ for the second half of the century. In this scenario, the effect
541 of a small amount of continued fossil fuel emissions is roughly balanced by other ^{14}C fluxes. The
542 less ambitious mitigation scenario SSP1-2.6 reaches a minimum of -38 ‰ in the 2050s and then
543 rebounds slightly. The simulated $\Delta^{14}CO_2$ for SSP1-2.6 is approximately 20 ‰ lower than the
544 simulated $\Delta^{14}CO_2$ for RCP2.6 in *Graven* [2015] due to the different structure of the model
545 biosphere, the different criteria for selecting model parameters, and differences between
546 emissions in SSP1-2.6 and RCP2.6 (see SM2).

547 The scenarios SSP2-4.5, SSP3-7.0 and SSP5-8.5 include the least mitigation of emissions and
548 simulated $\Delta^{14}CO_2$ declines steadily until late in the century. Atmospheric $\Delta^{14}CO_2$ reaches -105

549 ‰, -209 ‰ and -290 ‰ for SSP2-4.5, SSP3-7.0 and SSP5-8.5, respectively. SSP2-4.5 and
550 SSP3-7.0 are comparable to RCP4.5 and RCP8.5, which were simulated to reach -80 and -254 ‰
551 by *Graven* [2015]. In this case the differences in the model structure, calibration and scenario
552 cause $\Delta^{14}CO_2$ to be 25 ‰ lower or 40 ‰ higher $\Delta^{14}CO_2$ in 2100. The scenario SSP5-8.5 has
553 stronger emissions than any of the RCPs and therefore a more negative $\Delta^{14}CO_2$ in 2100.

554 In the overshoot scenario SSP5-3.4os, $\Delta^{14}CO_2$ is simulated to rebound quickly after 2050 due to
555 the reduction in fossil fuel emissions and the rapid implementation of BECCS. The input of
556 fossil carbon is rapidly reduced and the removal of lower-$\Delta^{14}C$ carbon, relative to the carbon in
557 the shallow ocean and terrestrial biosphere, leads to a net efflux of ^{14}C back to the atmosphere
558 that increases $\Delta^{14}CO_2$.

559
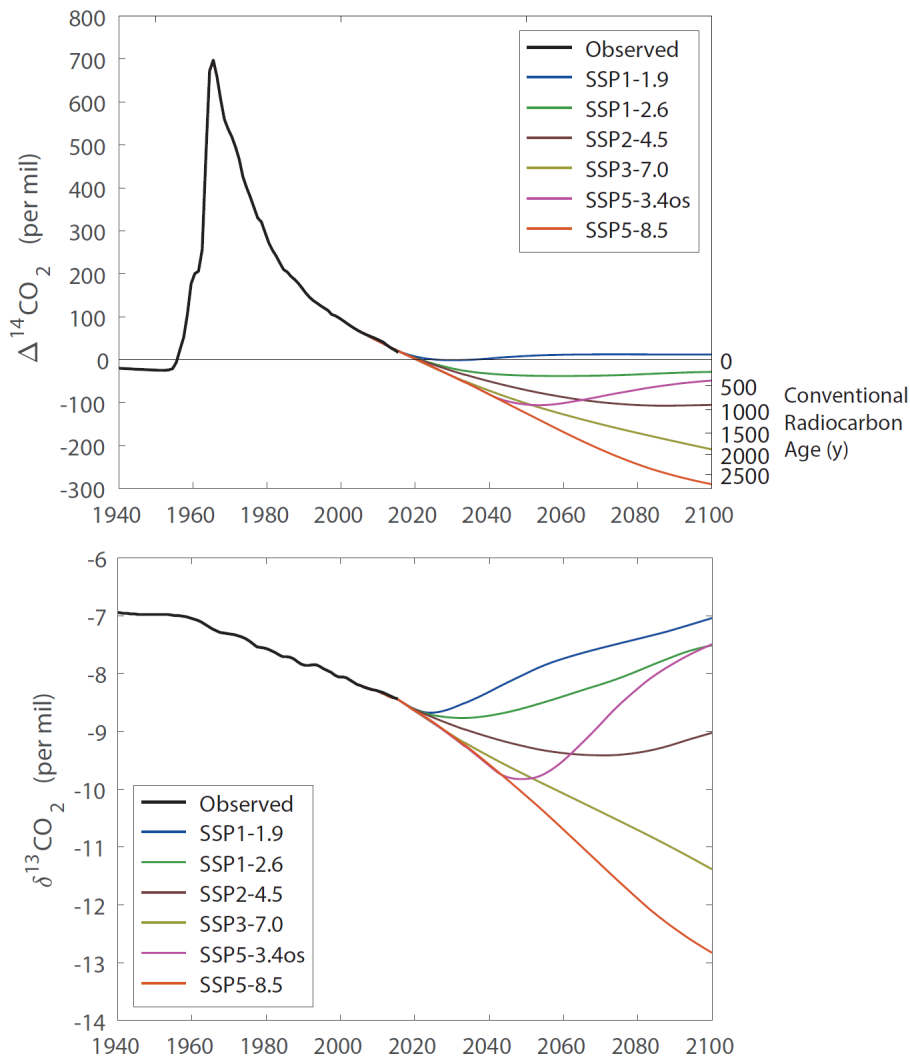
560

561 Figure 6: Observed $\Delta^{14}CO_2$ and $\delta^{13}CO_2$ for 1940 to 2015 and simulated $\Delta^{14}CO_2$ and $\delta^{13}CO_2$ for
562 2015 to 2100 for the six SSP-based CMIP6 ScenarioMIP scenarios. Colored lines show the mid-
563 range values across the 32 sets of parameters used in the simulations. The right axis in the top
564 panel shows the conventional radiocarbon age of a carbon-containing specimen with the same
565 radiocarbon content, calculated by 8033 * ln ($\Delta^{14}C/1,000 + 1$).

16

566

567   Simulated $\delta^{13}CO_2$ declines to approximately -8.7 ‰ in 2025 in all SSP-based scenarios and then
568   diverges. All scenarios that we explored that reach a peak and then reduce fossil fuel emissions
569   (all but SSP3-7.0 and SSP5-8.5) show an inflection in $\delta^{13}CO_2$ that is more pronounced than for
570      $\Delta^{14}CO_2$. In SSP1-1.9, $\delta^{13}CO_2$ is approximately -7 ‰ in 2100, about the same as it was in 1940.
571   SSP1-2.6 and SSP5-3.4os both have $\delta^{13}CO_2$ of approximately -7.5 ‰ in 2100, after a stronger
572   decline and reversal in SSP5-3.4os compared to SSP1-2.6. SSP2-4.5 reaches a minimum of -9.4
573   ‰ in 2070, then returns to -9 ‰ by 2100. SSP3-7.0 and SSP5-8.5 decrease through the century
574   and reach -11.4 ‰ and -12.8 ‰, respectively, in 2100.

575   In Figure 7, we show the individual contributions to the trends in $\delta^{13}CO_2$ and $\Delta^{14}CO_2$ for SSP1-
576   2.6, SSP5-3.4os and SSP5-8.5. The contributions for SSP1-1.9, SSP2-4.5 and SSP3-7.0 are
577   shown in Figure S1. Over the recent past, 2000-2015, the negative influence of the ocean
578   weakens from about -5 ‰ yr^{-1} to zero while the negative influence of fossil fuel emissions
579   strengthens slightly. Positive influences from biospheric exchange and from ^{14}C production by
580   natural cosmogenic radiation and by nuclear power plants have relatively constant positive
581   influences of 3-4 ‰ yr^{-1} over 2000-2015. Trend contributions of similar magnitudes were found
582   in the early 2000s by *Levin et al.* [2010] and *Graven et al.* [2012b].

583
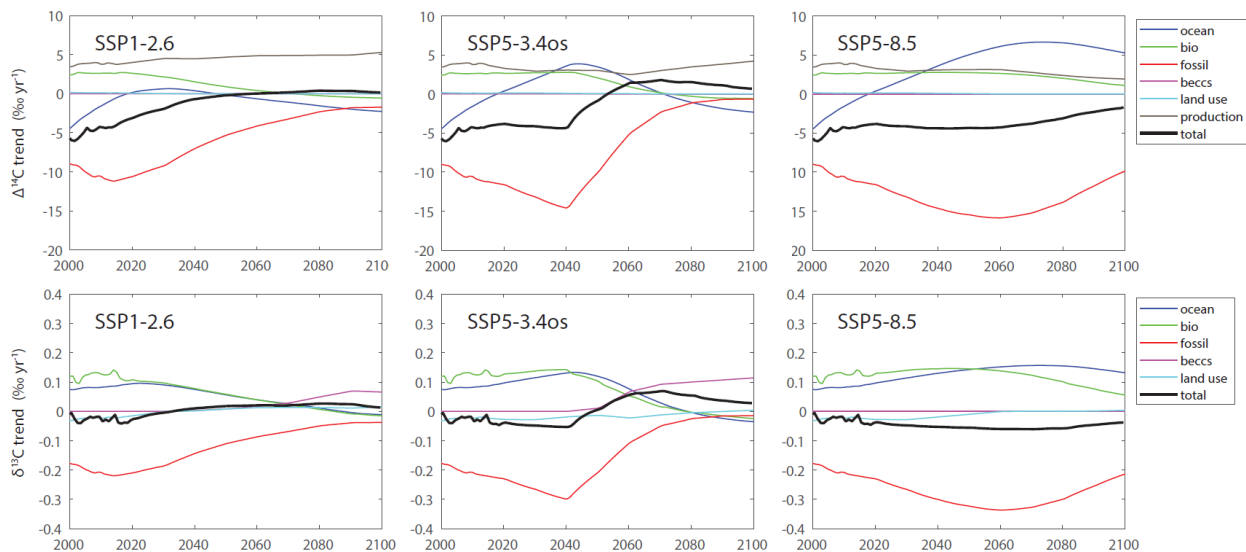
584

585   Figure 7: Simulated trend components for $\Delta^{14}CO_2$ (top row) and $\delta^{13}CO_2$ (bottom row) for SSP1-
586   2.6, SSP5-3.4os and SSP5-8.5. Other SSP-based scenarios are shown in Figure S1. Colored lines
587   show the mid-range values across the 32 sets of parameters used in the simulations. BECCS and
588   land use contributions are uniformly near zero for $\Delta^{14}CO_2$.

589

590   After 2015 the SSP scenarios diverge. The fossil fuel influence weakens in SSP1-2.6, followed
591   by an inflection in the oceanic and biospheric contributions, which turn negative around mid-
592   century. After this point, the positive influence of ^{14}C production is approximately balanced by
593   the other influences and $\Delta^{14}CO_2$ remains around -30 ‰ (Figure 6). In these simulations, nuclear
594   power plant ^{14}C emissions are assumed to stay constant at 2008 values throughout 2100. In

595   reality, these emissions could increase or decrease, depending on the future changes in the
596   nuclear industry. However, nuclear power plant ^{14}C emissions are only about 10% of natural ^{14}C
597   production so their changes are unlikely to have a large impact on these simulations. Even
598   though natural and nuclear power plant ^{14}C production is constant in the future simulations, its
599   contribution to the $\Delta^{14}CO_2$ trend varies over time and across different simulations because it
600   depends on the CO_2 concentration in the atmosphere. BECCS and land use have essentially no
601   effect on $\Delta^{14}CO_2$ in SSP1-2.6 or in any other SSP-based scenario assessed here.

602   For SSP5-3.4os and SSP5-8.5, the negative influence of fossil fuel emissions strengthens until
603   2040 (SSP5-3.4os) or 2060 (SSP5-8.5). Over this time, the overall trend in $\Delta^{14}CO_2$ remains
604   approximately steady at -4 ‰ yr^{-1}, which results from the change in oceanic influence
605   counteracting the strengthening in fossil fuel influence. Other influences remain steady. In 2040,
606   SSP5-3.4os begins a rapid reduction in fossil fuel emissions (Figure 5). About ten years later,
607    $\Delta^{14}CO_2$ starts to increase. The rapid weakening of the fossil fuel influence on $\Delta^{14}CO_2$ leads to a
608   net positive trend in $\Delta^{14}CO_2$ starting in the 2050s. This suggests that a rapid decarbonization of
609   the energy system could lead to the first increase in $\Delta^{14}CO_2$ since the "bomb peak" in 1964-65.
610   In contrast, the decreasing trend in SSP5-8.5 remains remarkably steady before weakening in the
611   last few decades of the century. In this scenario, the positive influence of ocean exchange
612   becomes twice as strong as the positive influence of ^{14}C production. The strong positive
613   influence from the ocean is a major reversal from the preindustrial period when the ocean was
614   the main negative influence counteracting natural ^{14}C production, and from the 20th century
615   period when the ocean was the main sink for bomb ^{14}C.

616   In all scenarios, the biospheric influence responds to the change in the atmospheric trend that
617   governs the biospheric disequilibrium. For example, as the $\Delta^{14}CO_2$ trend slows, the biospheric
618   disequilibrium weakens because Δ^{14}C of previously assimilated carbon is more similar to present
619    $\Delta^{14}CO_2$. Sign changes in the $\Delta^{14}CO_2$ trend lead to sign changes in the biospheric diequilibrium
620   and influence on the $\Delta^{14}CO_2$ trend. The effect is modulated by the turnover time of carbon in the
621   biosphere, between 36 and 56 years (Text SM2, [*Naegler and Levin*, 2009]). The oceanic
622   influence responds to changes in the $\Delta^{14}CO_2$ trend with a longer effective turnover time and with
623   exchanges between many vertical boxes.For $\delta^{13}CO_2$, the positive biospheric and oceanic
624   contributions to the trend nearly balance the negative fossil fuel contribution over 2000-2015.
625   The negative influence from land use is much smaller and similar to the overall trend. In SSP1-
626   2.6 fossil fuel emissions peak and slowly weaken after 2015, leading to a weaker negative trend
627   in $\delta^{13}CO_2$. Interestingly, the fossil fuel emissions in 2030 are not much smaller than 2015, but the
628   overall trend in $\delta^{13}CO_2$ is positive. The weakening in the biospheric and oceanic contributions
629   happens more slowly than for the fossil fuel contribution, resulting in an overall positive trend in
630    $\delta^{13}CO_2$ despite the continued fossil fuel emissions. This indicates the negative trend in $\delta^{13}CO_2$
631   that has been taken as an indication of the ^{13}C Suess Effect is actually dependent not just on the
632   presence of fossil fuel emissions but on the acceleration in fossil fuel emissions or their
633   magnitude. In SSP1-2.6 the effect of land use switches sign around 2030 but remains small.
634   After 2070, BECCS is the strongest positive contribution to the $\delta^{13}CO_2$ trend. The disequilibria
635   in the biosphere and ocean switch sign around 2080 after several decades of increasing $\delta^{13}CO_2$.

636   In SSP5-3.4os, the patterns are similar to SSP1-2.6 but more extreme as a result of the rapid drop
637   in fossil fuel emissions and the rapid expansion of BECCS. Between 2040 and 2060, the $\delta^{13}CO_2$
638   trend changes from about -0.05 ‰ yr^{-1} to more than +0.05 ‰ yr^{-1}. In SSP5-8.5, $\delta^{13}CO_2$ continues
639   to decrease even after fossil fuel emissions growth stalls in 2080, unlike the other two SSPs

640 where the $\delta^{13}CO_2$ trend turned positive after fossil fuel emissions weakened. In SSP5-8.5, the
641 fossil fuel emissions are large enough that the fossil fuel contribution to the $\delta^{13}CO_2$ trend remains
642 dominant.

643 The simulated future changes in atmospheric $\delta^{13}CO_2$ and $\Delta^{14}CO_2$ span a larger range than
644 previous atmospheric carbon isotope studies [*Graven*, 2015; *Köhler*, 2016]. This is expected
645 because the SSP-based scenarios span a larger range in atmospheric CO_2 concentration and fossil
646 fuel emissions than the RCPs. The lowest simulated $\Delta^{14}CO_2$ in 2100 for SSP5-8.5 is nearly -300
647 ‰ while the highest simulated $\Delta^{14}CO_2$ in 2100 for SSP1-1.9 is above 0 ‰. The range in the
648 RCPs was -250 to -20 ‰ [*Graven*, 2015]. For $\delta^{13}CO_2$, the lowest simulated value in 2100 for
649 SSP5-8.5 is nearly -13 ‰, while the highest simulated value in 2100 for SSP1-1.9 is
650 approximately 7 ‰, similar to what it was in 1950. It is difficult to compare these values with
651 [*Köhler*, 2016] because his simulations underestimated $\delta^{13}CO_2$ observed over the Industrial
652 Period.

653 We emphasize that these simulations do not account for all climate change-related feedbacks to
654 ^{13}C and ^{14}C fluxes. They do account for temperature-driven changes to solubility and
655 fractionation that affect air-sea exchanges, but not for other potential changes to ocean or
656 terrestrial biospheric fluxes. For example, *Khatiwala et al.* [2018] found that simulated changes
657 in ocean circulation affected the air-sea ^{14}C fluxes over the 21st century, although these fluxes
658 were still within the range simulated by *Graven* [2015]. Changes to ocean circulation could also
659 affect ^{13}C fluxes, and other changes such as wind speed not considered by *Khatiwala et al.*
660 [2018] could affect both ^{13}C and ^{14}C fluxes through the impact on gas exchange. On land,
661 changes in climate could affect photosynthesis, turnover of biospheric carbon, and permafrost
662 stability with impacts on ^{13}C and ^{14}C fluxes. However, we do expect that the SSP-driven changes
663 in emissions and atmospheric CO_2 concentration that are included in these simulations will be
664 the dominant influences over this century.

665

9. Impacts of Predicted Future Changes

667 The predicted changes in atmospheric $\delta^{13}CO_2$ and $\Delta^{14}CO_2$ have impacts on the way $\delta^{13}CO_2$ and
668 $\Delta^{14}CO_2$ are used in carbon cycle science and other fields. As described in *Graven* [2015] high
669 emissions scenarios that cause strong decreases in $\Delta^{14}CO_2$ provide a continuing atmospheric
670 perturbation that can be tracked to study exchange rates and residence times in different carbon
671 pools. However, these scenarios create problems for applications such as radiocarbon dating
672 because recently produced materials will have the same radiocarbon content as materials
673 produced at some point up to 2500 years in the past. Figure 6 includes on the right axis the
674 equivalent conventional radiocarbon age. This shows the age of materials with the same ratio of
675 $^{14}C/C$ but where the ratio has been reduced because of radioactive decay rather than dilution by
676 fossil carbon. The "age" of the atmosphere in the highest emission scenario is up to 2500 years in
677 the year 2100, older than for the highest RCP [*Graven*, 2015]. In this scenario, radiocarbon
678 dating would not be able to distinguish newly produced materials from those up to 2500 years
679 old by the end of this century and by 2050, radiocarbon dating would give ambiguous results for
680 samples up to nearly 1500 years old. These periods encompass much of the development of
681 human civilization when radiocarbon dating has been a key tool in archaeology.

682 Similarly, applications for forgery detection or illegal ivory trading will be affected because
683 newly produced materials will not be so easily distinguished from older ones. Radiocarbon

684 measurements have been used to date the age of ivory [*Cerling et al.*, 2016], with low
685 radiocarbon content below Modern reflecting ivory produced prior to the 1950s that is not
686 subject to legal restrictions or bans. But new ivory will soon also measure below 0 ‰,
687 eliminating the use of ^{14}C as a detection tool for illegal ivory. Within carbon cycle science, the
688 high emissions scenarios reduce the effectiveness of using $\Delta^{14}CO_2$ to quantify fossil fuel
689 emissions because the sensitivity of $\Delta^{14}CO_2$ to fossil fuel CO_2 goes down from -2.6‰ ppm^{-1}
690 presently to -1.6‰ ppm^{-1} in 2050 for high-emission scenarios [*Graven*, 2015]. Advances in
691 measurement precision are needed to maintain the detection limit for fossil fuel CO_2, but
692 measurement precision has not improved over the last 10 years.

693 On the other hand, low emission scenarios reduce the impact to these applications above but
694 create different challenges for other applications. Low emission scenarios cause $\Delta^{14}CO_2$ to
695 stabilize in the mid to late 21st century, eliminating the temporal change in $\Delta^{14}CO_2$ that formed
696 the basis of many applications examining exchange rates and residence times, both in carbon
697 cycle science and other field such as physiology. For example, in physiology the production of
698 different types of cells can be assessed with their radiocarbon content. The age of a person can be
699 matched to the atmospheric "bomb curve" (Figure 3) to determine what the $\Delta^{14}C$ in the cells of
700 interest would be at birth or early in life, and then by comparing the $\Delta^{14}C$ in cells of adults their
701 production rate be estimated [*Spalding et al.*, 2005]. If atmospheric $\Delta^{14}CO_2$ stabilizes, then this
702 application cannot be used because the difference in radiocarbon content of materials produced
703 in different years or decades would drop to very low levels. This type of application is now
704 widely used to examine decadal-scale carbon turnover in soil science [*Trumbore*, 2000] and it
705 would be difficult to replace with other methods.

706 For $\delta^{13}CO_2$, the predicted changes also have impacts on applications using atmospheric $\delta^{13}CO_2$
707 measurements. As atmospheric $\delta^{13}CO_2$ changes, the disequilibrium between atmospheric CO_2
708 and the carbon in the terrestrial biosphere and the ocean will also change. Following a low
709 emission scenario will result in the atmospheric $\delta^{13}CO_2$ trend reversing and the disequilibrium
710 changing sign. For atmospheric inversions interpreting atmospheric $\delta^{13}CO_2$, it will be important
711 to accurately estimate the changing disequilibrium flux despite potentially complex changes.
712 Studies of plant activity using tree rings could also be complicated by the reversal of the
713 atmospheric $\delta^{13}CO_2$ trend in the low emission scenarios, or by the predicted changes in
714 discrimination of several per mil in the high emission scenarios (Figure 5). Ocean observations
715 of $\delta^{13}C$ will also show a more complicated relationship with anthropogenic CO_2 in the low
716 emission scenarios, such that it may not be possible to use ocean $\delta^{13}C$ data to estimate ocean CO_2
717 uptake as it has been used in the past [*Gruber and Keeling*, 2001; *Quay et al.*, 2003].

718

10. Current Status and Future Needs for Observations and Modelling of Carbon Isotopes

720 Observations of $\delta^{13}C$ and $\Delta^{14}C$ in atmospheric CO_2 and other carbon reservoirs have enabled
721 important insights on the carbon cycle and on atmospheric and oceanic circulation, as outlined
722 above. The observations from the unique period of the nuclear bomb testing were particularly
723 powerful and scientific research would have benefitted greatly if an even larger number of
724 observations had been made during that time, across a larger variety of environments, including
725 additional measurements of the atmosphere and ocean as well as the carbon in soils, rivers and
726 lakes. The geochemist Wally Broecker, who pioneered many radiocarbon applications, used to

727 say, "Instead of publishing papers, we should have just dropped everything and collected
728 samples all over the world".

729 Another critical period is now upon us, as $\Delta^{14}CO_2$ drops below 0 ‰ and either stabilizes or
730 continues dropping to very low levels. Simulations of future atmospheric changes demonstrate
731 that it is unavoidable that some applications for $\Delta^{14}C$, and possibly $\delta^{13}C$, will become less
732 effective in the future. The specific applications that will be affected depend on the emissions
733 pathway followed. Since the utility of at least some applications is decreasing over time,
734 observations made now will, in general, be more useful than those that will be made in the
735 future. For example, the use of $\Delta^{14}C$ measurements to establish the decadal scale turnover of
736 terrestrial carbon pools will disappear in the future if $\Delta^{14}CO_2$ stabilizes. Therefore, it would be
737 immensely valuable to make concerted, coordinated efforts to conduct more observations of
738 $\Delta^{14}C$ in the Earth system as soon as possible. The sooner we make the observations, the more we
739 will achieve with them.

740 Currently, observations of atmospheric $\delta^{13}CO_2$ and $\Delta^{14}CO_2$ are conducted by several laboratories
741 operating global or regional networks of stations. Global networks for $\delta^{13}CO_2$ are operated by the
742 US National Oceanic and Atmospheric Administration (NOAA), Australia's Commonwealth
743 Scientific and Industrial Research Organisation (CSIRO) and Scripps Institution of
744 Oceanography (SIO). Only one global network for $\Delta^{14}CO_2$ is currently being operated, by the
745 University of Heidelberg, although other global networks have operated in the past [*Graven et*
746 *al.*, 2012a; *Nydal and Lövseth*, 1983]. There are regional networks for $\Delta^{14}CO_2$ and $\delta^{13}CO_2$ in
747 Europe as part of the Integrated Carbon Observing System (ICOS) and in North America by
748 NOAA and other laboratories. Urban-scale networks have also been developed [*Turnbull et al.*,
749 2015]. Most of these observations are publicly available, for example through the World Data
750 Centre for Greenhouse Gases (https://gaw.kishou.go.jp/) or the ICOS portal (https://www.icos-
751 cp.eu/).

752 Little is known about the current atmospheric distribution of $\Delta^{14}CO_2$ and $\delta^{13}CO_2$ away from the
753 surface. There have been some stratospheric observations of $\Delta^{14}CO_2$ conducted since the late
754 1980s [*Kanu et al.*, 2016; *Nakamura et al.*, 1994] but these comprise only a handful of vertical
755 profiles. NOAA conducts regular aircraft measurements of $\Delta^{14}CO_2$ in the troposphere at some
756 sites in North America (Estevan Point, Park Falls, Cape May and Portsmouth) and at a larger
757 network of sites for $\delta^{13}CO_2$[*Miller et al.*, 2012; *Sweeney et al.*, 2015]. Some other aircraft
758 measurements of $\delta^{13}CO_2$ have also been made, showing influences of biospheric exchange and
759 atmospheric mixing in the northern free troposphere and influences of the stratosphere in the
760 tropopause region [*Assonov et al.*, 2010; *Levin et al.*, 2002]. More observations from aircraft
761 would help to refine our understanding of $\delta^{13}CO_2$ and $\Delta^{14}CO_2$ variations through the atmosphere,
762 with applications for assessing biospheric fluxes, fossil fuel emissions and atmospheric transport.
763 The implementation of laboratory calibration recommendations and continued intercomparison
764 activities are needed to ensure that data from different labs can be combined [*WMO/IAEA*, 2016].

765 In addition to efforts expanding the observations of $\Delta^{14}C$ and $\delta^{13}C$ across the carbon cycle,
766 efforts to make modelling tools more openly available are needed to optimize the scientific
767 advances that can be made with $\Delta^{14}C$ and $\delta^{13}C$ observations. We believe that existing
768 observations are underutilized at present because isotopic modelling tools and expertise are not
769 widely available or widely used. Modelling of atmospheric $\delta^{13}CO_2$ and $\Delta^{14}CO_2$ is typically done
770 on a case-by-case basis. There is currently a lack of shared atmospheric modelling tools for
771 isotopic simulations. Models are used on global scales and on regional scales, ranging from box

772 models to high-resolution three-dimensional transport models [*Basu et al.*, 2016; *Keeling et al.*,
773 2017; *Peters et al.*, 2018]. To simulate atmospheric $\delta^{13}CO_2$ and $\Delta^{14}CO_2$, models or data-based
774 estimates of the carbon and isotopic fluxes from relevant processes are also needed. Here too,
775 various models and estimates of isotopic fluxes have been used in individual studies, but not
776 many of these are made available for other researchers. To provide modelled isotopic fluxes for
777 use by the community, and to promote isotopic modelling in general, it was recommended that
778 modelling groups in the latest Coupled Model Intercomparison Project activity (CMIP6)
779 simulate carbon isotopes in the land and ocean modules of their Earth System Models using a
780 specified atmospheric boundary condition (Figure 3, *Graven et al.* [2017], *Jones et al.* [2016],
781 *Orr et al.* [2017]). Only one model, CESM2, has so far included carbon isotopes in their CMIP6
782 simulations. It is hoped that the next phase of the CMIP will include more isotopic modeling, and
783 that isotopic modeling will be incorporated in other large modeling activities. Simulation of
784 atmospheric $\delta^{13}CO_2$ and $\Delta^{14}CO_2$ in the atmospheric models of Earth System Models has not yet
785 been implemented so it is currently not possible to do a fully coupled simulation of $\delta^{13}C$ and
786 $\Delta^{14}C$ using the most state-of-the-art models. Such fully coupled isotopic models would be useful
787 not only for the modern period, but also for paleoclimate modeling. Other shared tools enabling
788 atmospheric modeling of $\delta^{13}CO_2$ and $\Delta^{14}CO_2$ would also help to exploit existing and future
789 atmospheric measurements.

790 To fully develop the use of $\Delta^{14}CO_2$ observations to monitor regional emissions from fossil fuel
791 combustion, many more observations and better modeling capabilities on regional scales are
792 needed. Studies of dense regional atmospheric measurement networks combined with high
793 resolution atmospheric modeling have only recently been published [*Graven et al.*, 2018; Basu et
794 al. 2020] and best practices are still under development. For example, different studies have
795 constructed atmospheric inversions differently. The methods used in *Graven et al.* [2018] and
796 *Fischer et al.* [2017] first calculate fossil fuel derived CO_2 (ffCO_2, Equation 1) and biospheric
797 CO_2, and then run an inversion for fossil fuel and biospheric fluxes. In contrast, *Basu et al.*
798 [2016] set up their inversion to estimate individual $^{14}CO_2$ and CO_2 fluxes across North America,
799 including all the processes that can influence $\Delta^{14}CO_2$ in the inversion. Other best practices that
800 are still under development include the location and sampling height of observation sites in the
801 network. Sites that have lower sampling heights or that are located closer to emission sources
802 have higher signals in ffCO_2, whereas sites with higher sampling heights or located further from
803 sources have lower signals but they represent larger regions. Having more than one observation
804 site within a particular region can be important to prevent biases from any unique site
805 characteristics, for example including both urban and ex-urban sites that differ not only in their
806 ffCO_2 signals or representation scale but also in the atmospheric model's representation of the
807 transport in different types of regions [*Brophy et al.*, 2019]. In some locations, the ^{14}C emissions
808 from nuclear power plants can cause enrichment of $\Delta^{14}CO_2$, particularly near to high ^{14}C-
809 emitting reactors in the UK and Canada [*Bozhinova et al.*, 2014; *Graven and Gruber*, 2011;
810 *Vogel et al.*, 2013]. A better understanding of ^{14}C emissions from nuclear power plants and better
811 ^{14}C emissions data would enable their effect to be accurately accounted for and improve the
812 utility of $\Delta^{14}CO_2$ for ffCO_2 quantification in regions with nuclear power plants. Further
813 development of regional networks for $\Delta^{14}CO_2$ and complementary measurements including
814 satellite observations, as well as the model-data analysis frameworks for interpreting the
815 observations to constrain ffCO_2 emissions are needed [*Ciais et al.*, 2015; *Fischer et al.*, 2017].

816 **11. Summary**

817   Since the Industrial Revolution, the carbon isotopic composition of atmospheric CO_2 has
818   undergone dramatic changes as a result of human activities and the response of the natural
819   carbon cycle to them. The relative amount of atmospheric ^{14}C and ^{13}C in CO_2 has decreased
820   because of the addition of ^{14}C- and ^{13}C-depleted fossil carbon, while the nuclear bomb tests
821   increased ^{14}C in the atmosphere in the 1950s and 60s. Measurements of $\Delta^{14}CO_2$ and $\delta^{13}CO_2$ have
822   been used to make invaluable contributions to our knowledge of atmospheric mixing, air-sea gas
823   exchange, plant function, and fossil fuel emissions. As fossil fuel burning continues to grow, the
824   Suess Effect on ^{14}C and ^{13}C in CO_2 continues. However, lower emission scenarios would lead to
825   stabilized $\Delta^{14}CO_2$ and increases in $\delta^{13}CO_2$ over this century. The different paths described by the
826   SSP-based scenarios show that there is a wide range of possible changes to ^{14}C and ^{13}C of CO_2 in
827   the future. Researchers should be aware of the possible changes to ensure the continued utility of
828   ^{14}C and ^{13}C measurements of CO_2 for scientific applications across various fields. We
829   recommend a concerted effort to increase the number of ^{14}C and ^{13}C measurements across the
830   Earth System and more development of publicly available modelling tools that incorporate ^{14}C
831   and ^{13}C, including Earth System Models.

Acknowledgments

842

843
844

845

References

847

Allison, C. E., and R. J. Francey (2007), Verifying Southern Hemisphere trends in atmospheric carbon dioxide stable isotopes, J Geophys Res, 112, D21304, doi: doi:10.1029/2006jd007345.

Andres, R. J., T. A. Boden, and G. Marland (2016), Annual Fossil-Fuel CO2 Emissions: Global Stable Carbon Isotopic Signature, edited, Carbon Dioxide Information Analysis Center, Oak Ridge National Laboratory, U.S. Department of Energy, Oak Ridge, Tenn., U.S.A.

Andres, R. J., G. Marland, T. Boden, and S. Bischof (2000), Carbon Dioxide Emissions from Fossil Fuel Consumption and Cement Manufacture, 1751-1991, and an Estimate of their Isotopic Composition and Latitudinal Distribution, in The Carbon Cycle, edited by T. W. a. D. Schimel, Cambridge University Press, Aspen, Colorado.

Assonov, S. S., C. A. M. Brenninkmeijer, T. J. Schuck, and P. Taylor (2010), Analysis of ^{13}C and ^{18}O isotope data of CO_2 in CARIBIC aircraft samples as tracers of upper troposphere/lower stratosphere mixing and the global carbon cycle, Atmospheric Chemistry and Physics, 10(17), 8575-8599, doi: 10.5194/acp-10-8575-2010.

Bastos, A., P. Ciais, J. Barichivich, L. Bopp, V. Brovkin, T. Gasser, S. Peng, J. Pongratz, N. Viovy, and C. M. Trudinger (2016), Re-evaluating the 1940s CO2 plateau, Biogeosciences, 13(17), 4877-4897, doi: 10.5194/bg-13-4877-2016.

Basu, S., J. B. Miller, and S. Lehman (2016), Separation of biospheric and fossil fuel fluxes of CO_2 by atmospheric inversion of CO_2 and $^{14}CO_2$ measurements: Observation System Simulations, Atmos. Chem. Phys., 16(9), 5665-5683, doi: 10.5194/acp-16-5665-2016.

Basu, S., S. J. Lehman, J. B. Miller, A. E. Andrews, C. Sweeney, K. R. Gurney, X. Xu, J. Southon, and P. P. Tans (2020), Estimating US fossil fuel CO_2 emissions from measurements of ^{14}C in atmospheric CO_2, Proceedings of the National Academy of Sciences, 117(24), 13300-13307, doi: 10.1073/pnas.1919032117.

Bauska, T. K., F. Joos, A. C. Mix, R. Roth, J. Ahn, and E. J. Brook (2015), Links between atmospheric carbon dioxide, the land carbon reservoir and climate over the past millennium, Nature Geosci, 8(5), 383-387, doi: 10.1038/ngeo2422.

Bowling, D. R., D. E. Pataki, and J. T. Randerson (2008), Carbon isotopes in terrestrial ecosystem pools and CO2 fluxes, New Phytol, 178(1), 24-40, doi: 10.1111/j.1469-8137.2007.02342.x.

Bowling, D. R., N. G. McDowell, B. J. Bond, B. E. Law, and J. R. Ehleringer (2002), 13C content of ecosystem respiration is linked to precipitation and vapor pressure deficit, Oecologia, 131(1), 113-124, doi: 10.1007/s00442-001-0851-y.

Bozhinova, D., M. K. van der Molen, I. R. van der Velde, M. C. Krol, S. van der Laan, H. A. J. Meijer, and W. Peters (2014), Simulating the integrated summertime $\Delta^{14}CO_2$ signature from anthropogenic emissions over Western Europe, Atmos. Chem. Phys., 14(14), 7273-7290, doi: 10.5194/acp-14-7273-2014.

Brand, W. A., L. Huang, H. Mukai, A. Chivulescu, J. M. Richter, and M. Rothe (2009), How well do we know VPDB? Variability of δ13C and δ18O in CO2 generated from NBS19-calcite, Rapid Communications in Mass Spectrometry, 23(6), 915-926, doi: 10.1002/rcm.3940.

Broecker, W. S., T.-H. Peng, G. Ostlund, and M. Stuiver (1985), The distribution of bomb radiocarbon in the ocean, Journal of Geophysical Research: Oceans, 90(C4), 6953-6970, doi: 10.1029/JC090iC04p06953.

Bronk Ramsey, C. (2008), Radiocarbon Dating: Revolutions in Understanding, Archaeometry, 50(2), 249-275, doi: 10.1111/j.1475-4754.2008.00394.x.

Brophy, K., H. Graven, A. J. Manning, E. White, T. Arnold, M. L. Fischer, S. Jeong, X. Cui, and M. Rigby (2019), Characterizing uncertainties in atmospheric inversions of fossil fuel CO2 emissions in California, Atmos. Chem. Phys., 19(5), 2991-3006, doi: 10.5194/acp-19-2991-2019.

Caldeira, K., G. H. Rau, and P. B. Duffy (1998), Predicted net efflux of radiocarbon from the ocean and increase in atmospheric radiocarbon content, Geophys Res Lett, 25(20), 3811-3814.

Cerling, T. E., J. E. Barnette, L. A. Chesson, I. Douglas-Hamilton, K. S. Gobush, K. T. Uno, S. K. Wasser, and X. Xu (2016), Radiocarbon dating of seized ivory confirms rapid decline in African elephant populations and provides insight into illegal trade, Proceedings of the National Academy of Sciences, 113(47), 13330-13335, doi: 10.1073/pnas.1614938113.

Ciais, P., D. Crisp, H. D. van der Gon, R. Engelen, G. Janssens-Maenhout, M. Heimann, P. Rayner, and M. Scholze (2015), Towards a European Operational Observing System to Monitor Fossil CO2 Emissions: Report from the expert group*Rep.*, European Commission, Brussels, Belgium.

899 Ciais, P., P. P. Tans, J. W. C. White, M. Trolier, R. J. Francey, J. A. Berry, D. R. Randall, P. J. Sellers, J. G. Collatz,
900 and D. S. Schimel (1995), Partitioning of ocean and land uptake of CO_2 as inferred by δ13C measurements from the
901 NOAA Climate Monitoring and Diagnostics Laboratory Global Air Sampling Network, Journal of Geophysical
902 Research: Atmospheres, 100(D3), 5051-5070, doi: 10.1029/94JD02847.
903 DeNiro, M. J., and S. Epstein (1978), Influence of diet on the distribution of carbon isotopes in animals, Geochimica
904 et Cosmochimica Acta, 42(5), 495-506, doi: https://doi.org/10.1016/0016-7037(78)90199-0.
905 Drake, T. W., et al. (2019), Mobilization of aged and biolabile soil carbon by tropical deforestation, Nature
906 Geoscience, 12(7), 541-546, doi: 10.1038/s41561-019-0384-9.
907 Eide, M., A. Olsen, U. S. Ninnemann, and T. Johannessen (2017), A global ocean climatology of preindustrial and
908 modern ocean δ13C, Global Biogeochemical Cycles, n/a-n/a, doi: 10.1002/2016GB005473.
909 Enting, I. G., C. M. Trudinger, and R. J. Francey (1995), A synthesis inversion of the concentration and δ 13 C of
910 atmospheric CO 2, Tellus B, 47(1-2).
911 Fischer, M. L., et al. (2017), Simulating estimation of California fossil fuel and biosphere carbon dioxide exchanges
912 combining in situ tower and satellite column observations, J Geophys Res-Atmos, 122(6), 3653-3671, doi:
913 10.1002/2016jd025617.
914 Frank, D. C., et al. (2015), Water-use efficiency and transpiration across European forests during the Anthropocene,
915 Nature Clim. Change, 5(6), 579-583, doi: 10.1038/nclimate2614
916 http://www.nature.com/nclimate/journal/v5/n6/abs/nclimate2614.html#supplementary-information.
917 Friedli, H., H. Lötscher, H. Oeschger, U. Siegenthaler, and B. Stauffer (1986), Ice core record of the 13C/12C ratio
918 of atmospheric CO2 in the past two centuries, Nature, 324, 237, doi: 10.1038/324237a0.
919 Geyh, M. A. (2001), Bomb Radiocarbon Dating Of Animal Tissues And Hair, Radiocarbon, 43(2B), 723-730.
920 Graven, H., et al. (2017), Compiled records of carbon isotopes in atmospheric CO_2 for historical simulations in
921 CMIP6, Geosci. Model Dev., 10(12), 4405-4417, doi: 10.5194/gmd-10-4405-2017.
922 Graven, H., et al. (2018), Assessing fossil fuel CO_2 emissions in California using atmospheric observations and
923 models, Environmental Research Letters, 13(6), 065007.
924 Graven, H. D. (2015), Impact of fossil fuel emissions on atmospheric radiocarbon and various applications of
925 radiocarbon over this century, P Natl Acad Sci USA, 112(31), 9542-9545, doi: doi:10.1073/pnas.1504467112.
926 Graven, H. D., and N. Gruber (2011), Continental-scale enrichment of atmospheric $^{14}CO_2$ from the nuclear power
927 industry: Potential impact on the estimation of fossil fuel-derived CO_2, Atmospheric Chemistry and Physics, 11(23),
928 12339-12349, doi: 10.5194/acp-11-12339-2011.
929 Graven, H. D., T. P. Guilderson, and R. F. Keeling (2012a), Observations of radiocarbon in CO_2 at seven global
930 sampling sites in the Scripps flask network: Analysis of spatial gradients and seasonal cycles, J Geophys Res,
931 117(D2), D02303, doi: doi:10.1029/2011JD016535.
932 Graven, H. D., T. P. Guilderson, and R. F. Keeling (2012b), Observations of radiocarbon in CO_2 at La Jolla,
933 California, USA 1992-2007: Analysis of the long-term trend, J Geophys Res, 117(D2), D02302, doi:
934 doi:10.1029/2011JD016533.
935 Graven, H. D., N. Gruber, R. Key, S. Khatiwala, and X. Giraud (2012c), Changing controls on oceanic radiocarbon:
936 New insights on shallow-to-deep ocean exchange and anthropogenic CO_2 uptake, J Geophys Res, 117, C10005, doi:
937 doi:10.1029/2012JC008074.
938 Gruber, N., and C. D. Keeling (2001), An improved estimate of the isotopic air-sea disequilibrium of CO2:
939 Implications for the oceanic uptake of anthropogenic CO2, Geophysical Research Letters, 28(3), 555-558, doi:
940 10.1029/2000GL011853.
941 Hammer, S., et al. (2017), Compatibility of Atmospheric 14CO2 Measurements: Comparing the Heidelberg Low-
942 Level Counting Facility to International Accelerator Mass Spectrometry (AMS) Laboratories, Radiocarbon, 59(3),
943 875-883, doi: 10.1017/RDC.2016.62.
944 Hesshaimer, V., M. Heimann, and I. Levin (1994), Radiocarbon evidence for a smaller oceanic carbon dioxide sink
945 than previously believed, Nature, 370(6486), 201-203.
946 Hoesly, R. M., et al. (2018), Historical (1750–2014) anthropogenic emissions of reactive gases and aerosols from
947 the Community Emissions Data System (CEDS), Geosci. Model Dev., 11(1), 369-408, doi: 10.5194/gmd-11-369-
948 2018.
949 Hogg, A. G., et al. (2013), SHCal13 Southern Hemisphere Calibration, 0-50,000 Years Cal BP, Radiocarbon, 55(4),
950 1889-1903, doi: doi:10.2458/azu_js_rc.55.16783.
951 Jones, C. D., et al. (2016), C4MIP – The Coupled Climate–Carbon Cycle Model Intercomparison Project:
952 experimental protocol for CMIP6, Geosci Model Dev, 9(8), 2853-2880, doi: doi:10.5194/gmd-9-2853-2016.

953   Kanu, A. M., L. L. Comfort, T. P. Guilderson, P. J. Cameron-Smith, D. J. Bergmann, E. L. Atlas, S. Schauffler, and
954   K. A. Boering (2016), Measurements and modeling of contemporary radiocarbon in the stratosphere, Geophysical
955   Research Letters, 43(3), 1399-1406, doi: 10.1002/2015GL066921.

956   Keeling, C. D. (1958), The concentration and isotopic abundances of atmospheric carbon dioxide in rural areas,
957   Geochimica et Cosmochimica Acta, 13(4), 322-334, doi: https://doi.org/10.1016/0016-7037(58)90033-4.

958   Keeling, C. D. (1960), The Concentration and Isotopic Abundances of Carbon Dioxide in the Atmosphere, Tellus,
959   12(2), 200-203.

960   Keeling, C. D. (1979), The Suess effect: ^{13}Carbon-^{14}Carbon interrelations, Environment Int, 2(4), 229-300, doi:
961   doi:10.1016/0160-4120(79)90005-9.

962   Keeling, C. D., T. P. Whorf, M. Wahlen, and J. van der Plichtt (1995), Interannual extremes in the rate of rise of
963   atmospheric carbon dioxide since 1980, Nature, 375(6533), 666-670.

964   Keeling, C. D., S. C. Piper, R. B. Bacastow, M. Wahlen, T. P. Whorf, M. Heimann, and H. A. Meijer (2005),
965   Atmospheric CO_2 and $^{13}CO_2$ exchange with the terrestrial biosphere and oceans from 1978 to 2000: observations
966   and carbon cycle implications, Springer Verlag, New York.

967   Keeling, C. D., R. Bacastow, A. Carter, S. Piper, T. P. Whorf, M. Heimann, W. G. Mook, and H. Roeloffzen (1989),
968   A three-dimensional model of atmospheric CO_2 transport based on observed winds: 1. Analysis of observational
969   data, Aspects of Climate Variability in the Pacific and the Western Americas, Geophys. Monogr. Ser, 55, 165-236.

970   Keeling, R. F., H. D. Graven, L. R. Welp, L. Resplandy, J. Bi, S. C. Piper, Y. Sun, A. Bollenbacher, and H. A. J.
971   Meijer (2017), Atmospheric evidence for a global secular increase in carbon isotopic discrimination of land
972   photosynthesis, Proceedings of the National Academy of Sciences, doi: 10.1073/pnas.1619240114.

973   Khatiwala, S., H. Graven, S. Payne, and P. Heimbach (2018), Changes to the Air-Sea Flux and Distribution of
974   Radiocarbon in the Ocean Over the 21st Century, Geophysical Research Letters, 45(11), 5617-5626, doi:
975   doi:10.1029/2018GL078172.

976   Köhler, P. (2016), Using the Suess effect on the stable carbon isotope to distinguish the future from the past in
977   radiocarbon, Environmental Research Letters, 11(12), 124016.

978   Krakauer, N. Y., J. T. Randerson, F. W. Primeau, N. Gruber, and D. Menemenlis (2006), Carbon isotope evidence
979   for the latitudinal distribution and wind speed dependence of the air?sea gas transfer velocity, Tellus B, 58(5), 390-
980   417, doi: 10.1111/j.1600-0889.2006.00223.x.

981   LaFranchi, B. W., et al. (2016), Strong regional atmospheric 14C signature of respired CO2 observed from a tall
982   tower over the midwestern United States, Journal of Geophysical Research: Biogeosciences, 121(8), 2275-2295, doi:
983   10.1002/2015JG003271.

984   Lal, D., and Rama (1966), Characteristics of global tropospheric mixing based on man-made C14, H3, and Sr90,
985   Journal of Geophysical Research, 71(12), 2865-2874, doi: 10.1029/JZ071i012p02865.

986   Levin, I., and V. Hesshaimer (2000), Radiocarbon – A Unique Tracer of Global Carbon Cycle Dynamics,
987   Radiocarbon, 42(1), 69-80.

988   Levin, I., J. Schuchard, B. Kromer, and K. O. Munnich (1989), The Continental European Suess Effect,
989   Radiocarbon, 31(3), 431-440.

990   Levin, I., B. Kromer, M. Schmidt, and H. Sartorius (2003), A novel approach for independent budgeting of fossil
991   fuel CO_2 over Europe by $^{14}CO_2$ observations, Geophysical Research Letters, 30(23), doi: 10.1029/2003gl018477.

992   Levin, I., S. Hammer, E. Eichelmann, and F. R. Vogel (2011), Verification of greenhouse gas emission reductions:
993   the prospect of atmospheric monitoring in polluted areas, Philosophical Transactions of the Royal Society of
994   London A: Mathematical, Physical and Engineering Sciences, 369(1943), 1906-1924, doi: 10.1098/rsta.2010.0249.

995   Levin, I., T. Naegler, B. Kromer, M. Diehl, R. J. Francey, A. J. Gomez-Pelaez, L. P. Steele, D. Wagenbach, R.
996   Weller, and D. E. Worthy (2010), Observations and modelling of the global distribution and long-term trend of
997   atmospheric $^{14}CO_2$, Tellus B, 62(1), 26-46.

998   Levin, I., et al. (2002), Three years of trace gas observations over the EuroSiberian domain derived from aircraft
999   sampling — a concerted action, Tellus B, 54(5), 696-712, doi: 10.1034/j.1600-0889.2002.01352.x.

1000   Lin, G., and J. R. Ehleringer (1997), Carbon Isotopic Fractionation Does Not Occur during Dark Respiration in C3
1001   and C4 Plants, Plant Physiol, 114(1), 391-394, doi: 10.1104/pp.114.1.391.

1002   Marwick, T. R., F. Tamooh, C. R. Teodoru, A. V. Borges, F. Darchambeau, and S. Bouillon (2015), The age of
1003   river-transported carbon: A global perspective, Global Biogeochemical Cycles, 29(2), 122-137, doi:
1004   10.1002/2014gb004911.

1005   Meinshausen, M., et al. (2011), The RCP greenhouse gas concentrations and their extensions from 1765 to 2300,
1006   Climatic Change, 109(1-2), 213-241, doi: 10.1007/s10584-011-0156-z.

1007   Meinshausen, M., et al. (2017), Historical greenhouse gas concentrations for climate modelling (CMIP6), Geosci
1008   Model Dev, 10(5), 2057-2116, doi: doi:10.5194/gmd-10-2057-2017.

1009   Miller, J., et al. (2013), Initial Results of an Intercomparison of AMS-Based Atmospheric $^{14}CO_2$ Measurements,
1010   Radiocarbon, 55(2-3), 1475-1483.
1011   Miller, J. B., and P. P. Tans (2003), Calculating isotopic fractionation from atmospheric measurements at various
1012   scales, Tellus B, 55(2), 207-214, doi: 10.1034/j.1600-0889.2003.00020.x.
1013   Miller, J. B., et al. (2012), Linking emissions of fossil fuel CO_2 and other anthropogenic trace gases using
1014   atmospheric $^{14}CO_2$, Journal of Geophysical Research, 117(D8), doi: 10.1029/2011jd017048.
1015   Naegler, T., and I. Levin (2006), Closing the global radiocarbon budget 1945–2005, J Geophys Res, 111(D12),
1016   D12311, doi: doi:10.1029/2005jd006758.
1017   Naegler, T., and I. Levin (2009), Biosphere-atmosphere gross carbon exchange flux and the $\delta^{13}CO_2$ and $\Delta^{14}CO_2$
1018   disequilibria constrained by the biospheric excess radiocarbon inventory, J Geophys Res, 114(D17), D17303, doi:
1019   doi:10.1029/2008jd011116.
1020   Naegler, T., P. Ciais, K. Rodgers, and I. Levin (2006), Excess radiocarbon constraints on air-sea gas exchange and
1021   the uptake of CO_2 by the oceans, Geophysical Research Letters, 33(11), doi: 10.1029/2005gl025408.
1022   Nakamura, T., T. Nakazawa, H. Honda, H. Kitagawa, T. Machida, A. Ikeda, and E. Matsumoto (1994), Seasonal
1023   variations in 14C concentrations of stratospheric CO2 measured with accelerator mass spectrometry, Nuclear
1024   Instruments and Methods in Physics Research Section B: Beam Interactions with Materials and Atoms, 92(1), 413-
1025   416, doi: https://doi.org/10.1016/0168-583X(94)96045-3.
1026   Newman, S., et al. (2016), Toward consistency between trends in bottom-up CO_2 emissions and top-down
1027   atmospheric measurements in the Los Angeles megacity, Atmos. Chem. Phys., 16(6), 3843-3863, doi: 10.5194/acp-
1028   16-3843-2016.
1029   Nydal, R. (1966), Variation in C^{14} concentration in the atmosphere during the last several years, Tellus, 18(2-3),
1030   271-279, doi: 10.1111/j.2153-3490.1966.tb00237.x.
1031   Nydal, R., and K. Lövseth (1983), Tracing Bomb ^{14}C in the Atmosphere, J Geophys Res, 88(C6), 3621-3642.
1032   O'Neill, B. C., et al. (2016), The Scenario Model Intercomparison Project (ScenarioMIP) for CMIP6, Geosci. Model
1033   Dev., 9(9), 3461-3482, doi: 10.5194/gmd-9-3461-2016.
1034   O'Neill, B. C., E. Kriegler, K. Riahi, K. L. Ebi, S. Hallegatte, T. R. Carter, R. Mathur, and D. P. van Vuuren (2014),
1035   A new scenario framework for climate change research: the concept of shared socioeconomic pathways, Climatic
1036   Change, 122(3), 387-400, doi: 10.1007/s10584-013-0905-2.
1037   Olsen, A., et al. (2016), An internally consistent data product for the world ocean: the Global Ocean Data Analysis
1038   Project, version 2 (GLODAPv2), Earth Syst. Sci. Data Discuss., 2016, 1-78, doi: 10.5194/essd-2015-42.
1039   Orr, J. C., et al. (2017), Biogeochemical protocols and diagnostics for the CMIP6 Ocean Model Intercomparison
1040   Project (OMIP), Geosci Model Dev, 10(6), 2169-2199, doi: doi:10.5194/gmd-10-2169-2017.
1041   Pataki, D. E., T. Xu, Y. Q. Luo, and J. R. Ehleringer (2007), Inferring biogenic and anthropogenic carbon dioxide
1042   sources across an urban to rural gradient, Oecologia, 152(2), 307-322, doi: 10.1007/s00442-006-0656-0.
1043   Pataki, D. E., J. R. Ehleringer, L. B. Flanagan, D. Yakir, D. R. Bowling, C. J. Still, N. Buchmann, J. O. Kaplan, and
1044   J. A. Berry (2003), The application and interpretation of Keeling plots in terrestrial carbon cycle research, Global
1045   Biogeochemical Cycles, 17(1), doi: 10.1029/2001gb001850.
1046   Peters, W., et al. (2018), Increased water-use efficiency and reduced CO2 uptake by plants during droughts at a
1047   continental scale, Nature Geoscience, doi: 10.1038/s41561-018-0212-7.
1048   Quay, P., R. Sonnerup, T. Westby, J. Stutsman, and A. McNichol (2003), Changes in the $^{13}C/^{12}C$ of dissolved
1049   inorganic carbon in the ocean as a tracer of anthropogenic CO_2 uptake, Glob Biogeochem Cycles, 17(1), 1004, doi:
1050   doi:10.1029/2001gb001817.
1051   Rafelski, L. E., S. C. Piper, and R. F. Keeling (2009), Climate effects on atmospheric carbon dioxide over the last
1052   century, Tellus B, 61(5), 718-731, doi: 10.1111/j.1600-0889.2009.00439.x.
1053   Rafter, T. A., and G. J. Fergusson (1957), "Atom Bomb Effect"--Recent Increase of Carbon-14 Content of the
1054   Atmosphere and Biosphere, Science, 126(3273), 557-558.
1055   Randerson, J. T., I. G. Enting, E. A. G. Schuur, K. Caldeira, and I. Y. Fung (2002a), Seasonal and latitudinal
1056   variability of troposphere Δ14CO2: Post bomb contributions from fossil fuels, oceans, the stratosphere, and the
1057   terrestrial biosphere, Global Biogeochemical Cycles, 16(4), 59-51-59-19, doi: 10.1029/2002gb001876.
1058   Randerson, J. T., G. J. Collatz, J. E. Fessenden, A. D. Munoz, C. J. Still, J. A. Berry, I. Y. Fung, N. Suits, and A. S.
1059   Denning (2002b), A possible global covariance between terrestrial gross primary production and ^{13}C discrimination:
1060   Consequences for the atmospheric ^{13}C budget and its response to ENSO, Glob Biogeochem Cycles, 16(4), 1136,
1061   doi: doi:10.1029/2001gb001845.
1062   Rayner, P. J., I. G. Enting, R. J. Francey, and R. Langenfelds (1999), Reconstructing the recent carbon cycle from
1063   atmospheric CO2, δ13C and O2/N2 observations*, Tellus B, 51(2), 213-232, doi: 10.1034/j.1600-0889.1999.t01-1-
1064   00008.x.

1065   Reimer, P. J., et al. (2013), IntCal13 and Marine13 radiocarbon age calibration curves 0–50,000 years cal BP,
1066   Radiocarbon, 55(4), 1869–1887, doi: doi:10.2458/azu_js_rc.55.16947.
1067   Resplandy, L., R. F. Keeling, C. Rödenbeck, B. B. Stephens, S. Khatiwala, K. B. Rodgers, M. C. Long, L. Bopp,
1068   and P. P. Tans (2018), Revision of global carbon fluxes based on a reassessment of oceanic and riverine carbon
1069   transport, Nature Geoscience, 11(7), 504-509, doi: 10.1038/s41561-018-0151-3.
1070   Riahi, K., et al. (2017), The Shared Socioeconomic Pathways and their energy, land use, and greenhouse gas
1071   emissions implications: An overview, Global Environmental Change, 42(Supplement C), 153-168, doi:
1072   10.1016/j.gloenvcha.2016.05.009.
1073   Rodgers, K. B., et al. (2011), Interhemispheric gradient of atmospheric radiocarbon reveals natural variability of
1074   Southern Ocean winds, Clim Past, 7(4), 1123-1138, doi: doi:10.5194/cp-7-1123-2011.
1075   Rogelj, J., et al. (2018), Scenarios towards limiting global mean temperature increase below 1.5 °C, Nature Climate
1076   Change, doi: 10.1038/s41558-018-0091-3.
1077   Rozanski, K., I. Levin, J. Stock, R. E. Guevara Falcon, and F. Rubio (1995), Atmospheric $^{14}CO_2$ Variations in the
1078   Equatorial Region, Radiocarbon, 37(2), 509-515, doi: 10.1017/S003382220003099X.
1079   Rubino, M., et al. (2013), A revised 1000 year atmospheric δ^{13}C-CO_2 record from Law Dome and South Pole,
1080   Antarctica, J Geophys Res Atmos, 118(15), 8482-8499, doi: doi:10.1002/jgrd.50668.
1081   Scholze, M., P. Ciais, and M. Heimann (2008), Modeling terrestrial ^{13}C cycling: Climate, land use and fire, Glob
1082   Biogeochem Cycles, 22(1), GB1009, doi: doi:10.1029/2006gb002899.
1083   Schubert, B. A., and A. H. Jahren (2012), The effect of atmospheric CO2 concentration on carbon isotope
1084   fractionation in C3 land plants, Geochimica et Cosmochimica Acta, 96, 29-43, doi: doi:10.1016/j.gca.2012.08.003.
1085   Schubert, B. A., and A. H. Jahren (2015), Global increase in plant carbon isotope fractionation following the Last
1086   Glacial Maximum caused by increase in atmospheric pCO2, Geology, 43(5), 435-438, doi: 10.1130/g36467.1.
1087   Scott, E. M., G. T. Cook, and P. Naysmith (2010), The Fifth International Radiocarbon Intercomparison (VIRI): An
1088   Assessment of Laboratory Performance in Stage 3, Radiocarbon, 52(3), 859-865, doi:
1089   10.1017/S003382220004594X.
1090   Spalding, K. L., R. D. Bhardwaj, B. A. Buchholz, H. Druid, and J. Frisén (2005), Retrospective birth dating of cells
1091   in humans, Cell, 122(1), 133-143.
1092   Stuiver, M. (1983), International Agreements and the Use of the New Oxalic Acid Standard, Radiocarbon, 25(2),
1093   793-795, doi: 10.1017/S0033822200006159.
1094   Stuiver, M., and H. A. Polach (1977), Discussion: Reporting of ^{14}C Data, Radiocarbon, 19(3), 355-363.
1095   Stuiver, M., and P. D. Quay (1981), Atmospheric ^{14}C changes resulting from fossil fuel CO_2 release and cosmic ray
1096   flux variability, Earth Planet Sci Lett, 53, 349-362.
1097   Suess, H. E. (1955), Radiocarbon concentration in modern wood, Science, 122, 415-417.
1098   Sweeney, C., E. Gloor, A. R. Jacobson, R. M. Key, G. McKinley, J. L. Sarmiento, and R. Wanninkhof (2007),
1099   Constraining global air-sea gas exchange for CO_2 with recent bomb ^{14}C measurements, Glob Biogeochem Cycles,
1100   21(2), GB2015, doi: doi:10.1029/2006gb002784.
1101   Sweeney, C., et al. (2015), Seasonal climatology of CO2 across North America from aircraft measurements in the
1102   NOAA/ESRL Global Greenhouse Gas Reference Network, Journal of Geophysical Research: Atmospheres,
1103   120(10), 5155-5190, doi: 10.1002/2014JD022591.
1104   Tans, P. P., A. F. M. De Jong, and W. G. Mook (1979), Natural atmospheric 14C variation and the Suess effect,
1105   Nature, 280(5725), 826-828.
1106   Tipple, B. J., S. R. Meyers, and M. Pagani (2010), Carbon isotope ratio of Cenozoic CO_2: A comparative evaluation
1107   of available geochemical proxies, Paleoceanography, 25(3), doi: 10.1029/2009pa001851.
1108   Trudinger, C. M., I. G. Enting, P. J. Rayner, and R. J. Francey (2002), Kalman filter analysis of ice core data 2.
1109   Double deconvolution of CO2 and δ13C measurements, Journal of Geophysical Research: Atmospheres, 107(D20),
1110   ACH 5-1-ACH 5-24, doi: 10.1029/2001JD001112.
1111   Trudinger, C. M., I. G. Enting, R. J. Francey, D. M. Etheridge, and P. J. Rayner (1999), Long-term variability in the
1112   global carbon cycle inferred from a high-precision CO2 and δ13C ice-core record, Tellus B: Chemical and Physical
1113   Meteorology, 51(2), 233-248, doi: 10.3402/tellusb.v51i2.16276.
1114   Trumbore, S. E. (2000), Age of Soil Organic Matter and Soil Respiration: Radiocarbon Constraints on Belowground
1115   C Dynamics, Ecol Appl, 10(2), 399-411.
1116   Turnbull, J. C., J. B. Miller, S. J. Lehman, P. P. Tans, R. J. Sparks, and J. Southon (2006), Comparison of $^{14}CO_2$,
1117   CO, and SF_6 as tracers for recently added fossil fuel CO_2 in the atmosphere and implications for biological CO_2
1118   exchange, Geophysical Research Letters, 33(1), doi: 10.1029/2005gl024213.

1119   Turnbull, J. C., S. E. Mikaloff Fletcher, I. Ansell, G. Brailsford, R. Moss, M. Norris, and K. Steinkamp (2016), Sixty
1120   years of radiocarbon dioxide measurements at Wellington, New Zealand 1954 – 2014, Atmos Chem Phys Discuss,
1121   2016, 1-28, doi: doi:10.5194/acp-2016-1110.
1122   Turnbull, J. C., et al. (2015), Toward quantification and source sector identification of fossil fuel CO2 emissions
1123   from an urban area: Results from the INFLUX experiment, Journal of Geophysical Research: Atmospheres, 120(1),
1124   292-312, doi: 10.1002/2014JD022555.
1125   Turney, C. S. M., D. Wheeler, and A. R. Chivas (2006), Carbon isotope fractionation in wood during carbonization,
1126   Geochimica et Cosmochimica Acta, 70(4), 960-964, doi: https://doi.org/10.1016/j.gca.2005.10.031.
1127   Vaughn, B. H., C. U. Evans, J. W. C. White, C. J. Still, K. A. Masarie, and J. Turnbull (2010), Global Network
1128   Measurements of Atmospheric Trace Gas Isotopes, in Isoscapes: Understanding Movement, Pattern, and Process on
1129   Earth Through Isotope Mapping, edited by J. B. West, G. J. Bowen, T. E. Dawson and K. P. Tu, pp. 3-31, Springer
1130   Amsterdam, Netherlands.
1131   Vogel, F. R., I. Levin, and D. E. Worthy (2013), Implications for Deriving Regional Fossil Fuel CO_2 Estimates from
1132   Atmospheric Observations in a Hot Spot of Nuclear Power Plant $^{14}CO_2$ Emissions, Radiocarbon, 55(2-3), 1556-
1133   1572.
1134   Vogel, F. R., S. Hammer, A. Steinhof, B. Kromer, and I. Levin (2010), Implication of weekly and diurnal ^{14}C
1135   calibration on hourly estimates of CO-based fossil fuel CO_2 at a moderately polluted site in southwestern Germany,
1136   Tellus B, 62(5), 512-520.
1137   Wang, H., I. C. Prentice, T. F. Keenan, T. W. Davis, I. J. Wright, W. K. Cornwell, B. J. Evans, and C. Peng (2017),
1138   Towards a universal model for carbon dioxide uptake by plants, Nature Plants, 3(9), 734-741, doi: 10.1038/s41477-
1139   017-0006-8.
1140   Wanninkhof, R. (2014), Relationship between wind speed and gas exchange over the ocean revisited, Limnology
1141   and Oceanography: Methods, 12(6), 351-362, doi: 10.4319/lom.2014.12.351.
1142   Wehr, R., J. W. Munger, J. B. McManus, D. D. Nelson, M. S. Zahniser, E. A. Davidson, S. C. Wofsy, and S. R.
1143   Saleska (2016), Seasonality of temperate forest photosynthesis and daytime respiration, Nature, 534(7609), 680-683,
1144   doi: 10.1038/nature17966.
1145   Wendeberg, M., J. M. Richter, M. Rothe, and W. A. Brand (2013), Jena Reference Air Set (JRAS): a multi-point
1146   scale anchor for isotope measurements of CO_2 in air, Atmos Meas Tech, 6(3), 817-822, doi: doi:10.5194/amt-6-817-
1147   2013.
1148   WMO/IAEA (2003), 11th WMO/IAEA Meeting on Carbon Dioxide and Related Measurement Techniques, Tokyo,
1149   Japan, 25 – 28 September 2001*Rep.*, World Meteorological Organization, Global Atmosphere Watch.
1150   WMO/IAEA (2016), 18th WMO/IAEA Meeting on Carbon Dioxide, Other Greenhouse Gases and Related Tracers
1151   Measurement Techniques (GGMT-2015)*Rep.*, World Meteorological Organization, Global Atmosphere Watch.
1152   WMO/IAEA (2018), 19th WMO/IAEA Meeting on Carbon Dioxide, Other Greenhouse Gases and Related Tracers
1153   Measurement Techniques (GGMT-2017)*Rep.*, World Meteorological Organization, Global Atmosphere Watch.
1154   Zazzeri, G., E. Acuña Yeomans, and H. D. Graven (2018), Global and regional emissions of radiocarbon from
1155   nuclear power plants from 1972 to 2016, Radiocarbon, 1-15, doi: 10.1017/RDC.2018.42.
1156   Zhang, J., P. D. Quay, and D. O. Wilbur (1995), Carbon isotope fractionation during gas-water exchange and
1157   dissolution of CO2, Geochimica et Cosmochimica Acta, 59(1), 107-114, doi: http://dx.doi.org/10.1016/0016-
1158   7037(95)91550-D.
1159